CHANGES IN BMP AND EGFR SIGNALING COMPONENTS UNDERLIE THE EVOLUTION OF DROSOPHILA EGGSHELL MORPHOLOGIES

by

MATTHEW GENE NIEPIELKO

A dissertation submitted to the Graduate School – Camden

Rutgers, The State University of New Jersey

in partial fulfillment of the requirements

for the degree of

Doctor of Computational and Integrative Biology

Graduate Program in

Computational and Integrative Biology

written under the direction of

Dr. Nir Yakoby

and approved by

_____

Nir Yakoby

_____

Benedetto Piccoli

_____

Stanislav Y. Shvartsman

_____

CCIB Program Director

Camden, New Jersey

May, 2014

ABSTRACT OF THE THESIS

CHANGES IN BMP AND EGFR SIGNALING COMPONENTS UNDERLIE THE EVOLUTION OF DROSOPHILA EGGSHELL MORPHOLOGIES

By: MATTHEW GENE NIEPIELKO

Dissertation Director:

Dr. Nir Yakoby

A fundamental requirement for understanding the evolution of tissue morphogenesis involves exploring underlying changes in cell signaling amongst species. We used the magnificent diversity of *Drosophila* eggshell morphologies to investigate mechanisms guiding morphological variation. *Drosophila* eggshell structures, including the dorsal appendages (DAs) and the dorsal ridge (DR), are formed during oogenesis when a 2D monolayer of follicle cells (FCs) overlying the oocyte is instructed by numerous cell signaling pathways to form the eggshell. Here, we focus on the bone morphogenetic protein (BMP) signaling in reference to DAs formation, and the epidermal growth factor receptor (EGFR) in reference to DR formation. BMP signaling in the FCs is initiated when the anteriorly secreted transforming growth factor-β-like Decepentaplegic (DPP) activates a uniform and then patterned type I BMP receptor Thickveins (TKV). We found that the pattern of BMP signaling is dynamic and spatially diverse in species with different DAs morphologies. Using computational modeling and experimental validation, we found that qualitative and quantitative changes in TKV can account for different BMP signaling outputs across species. The DR is a lumen-like structure along the dorsal-most side on eggshells of numerous species and absent from *D. melanogaster* eggshells. We developed a binary matrix to analyze 180 2D expression

patterns of a family of structural proteins, the Chorion proteins, in species with and without a DR and associate DR patterns to domains of known regulation. The DR domain clusters with EGFR regulated domains and thus, we focused on EGFR and DR formation. EGFR activation begins when the transforming growth factor-α-like ligand, Gurken (GRK), is secreted from the oocyte and creates a dorsal-ventral activation gradient. We found that DR morphologies correlate with EGFR signaling and GRK patterns in the DR domain. In the DR species *D. willistoni*, we successfully perturbed EGFR signaling and DR formation by genetically perturbing GRK levels. Expression of *D. willistoni* GRK (*w*GRK) in *D. melanogaster* rescues the GRK null phenotype and in some cases, *w*GRK is sufficient to produce a ridge-like structure on *D. melanogaster* eggshells. Our results support the idea that changes in major components of developmental pathways underlie the evolution of morphologies.

DEDICATION

I would like to dedicate this work to all my friends and family. Witnessing their accomplishments and hearing their words of encouragement gave me so much motivation and creativity. Thanks to their inspiration, this work was made possible.

ACKNOWLEDGEMENTS

I am extremely thankful for my advisor Nir Yakoby. Through his mentoring and friendship, Nir has given me tremendous amounts of experimental and analytical skills. Thanks to his leadership and encouragement, I have learned so much and have become the best possible scientist I can be. I would also like to thank my committee members, Professor Benedetto Piccoli and Professor Stanislav Y. Shvartsman. Their suggestions and inputs not only helped guide my research projects, but also helped broaden my approach to biological problems. The combined support from Nir, Dr. Piccoli, and Dr. Shvartsman has opened a wealth of opportunities for which I will be forever grateful.

A huge thanks to Kuhn Ip, Jitendra S. Kanodia, and Professor Desmond Lun for contributing their exceptional mathematical modeling abilities which resulted in successful predictions that were used for experimental design. I am incredibly grateful to Kenneth Kim, David Luor, and Chelsea Ray for their remarkable efforts that provided exciting results and experimental direction. A special thanks to Robert Marmion for being a wonderful friend and for his collaboration and matrix analyses which significantly enhanced this project. I am also appreciative for the friendship, support, and fruitful discussions from David Lemon, Nicole Pope, Steve Brownstein, Vikrant Singh, Dan Ricketti, and all the other members of the Yakoby Lab.

My research has enormously benefitted from the generosity of the *Drosophilia* community. I would like to thank D. Stern, F. Hassinger, C. Berg, H. Cui, L. Riddiford, M. O'Connor, J. Duffy, and T. Schüpbach, for graciously providing fly stocks and D. Vasiliauskas, S. Morton, T. Jessell, and E. Laufer for providing the P-SMAD antibody. I am also thankful for Primmbiotech, the VDRC, DSHB, Hybridoma Bank, and the UC *Drosophila* Stock Center for *Drosophila* fly species, stocks, and reagents. I

appreciate and recognize Rainbow Transgenics for successfully transforming *D. willistoni* after many attempts and thank Genetic Services for the *D. melanogaster* transformations. I greatly appreciate L. Cheung and the Princeton University Imaging Core Facility for the use of the Leica SP5 confocal microscope and Professor W. Saidel for his help with SEM imaging.

My work has been supported by grants and I thank the various sources including the Center for Computational and Integrative Biology at Rutgers-Camden, the Rutgers Faculty Research Grant (281715), and the NIH-National Institute of General Medical Sciences Award (R15GM101597) granted to Nir Yakoby.

Lastly, I am extremely thankful for the loving support from my family, especially my dear wife Angela. Without Angela's ongoing love, encouragement, and confidence in me, my research would simply not be possible.

TABLE OF CONTENTS

CHAPTERS

LIST OF FIGURES

Chapter 1:

Introduction

Morphology is a highly diverse trait in nature. A classical morphological diversity example is the beaks of Darwin's finches, which have evolved in size and shape to accommodate the utilization of specialized food sources (Abzhanov et al., 2004). While morphologies differ among animals, the molecular mechanisms controlling such changes are mostly unknown (Carroll, 2005, 2008). Using the remarkable morphological differences displayed by the eggshells of *Drosophila* species (Hinton, 1981; Kagesawa et al., 2008; Nakamura and Matsuno, 2003; Niepielko et al., 2011), we address fundamental questions surrounding the underlying mechanisms guiding the evolution of morphology.

1.1 *Drosophila* eggshell morphologies

The *Drosophila melanogaster* eggshell surrounds and shelters the developing embryo. It contains several functional structures, including the tube-like dorsal appendages (DAs) that allow for gas exchange between the developing embryo and the environment, the operculum, an opening for larva hatching, the posterior aeropyle that also functions in gas exchange, and the micropyle, a point of sperm entry (Fig. 1) (Berg, 2008; Ward and Berg, 2005)).

Figure 1

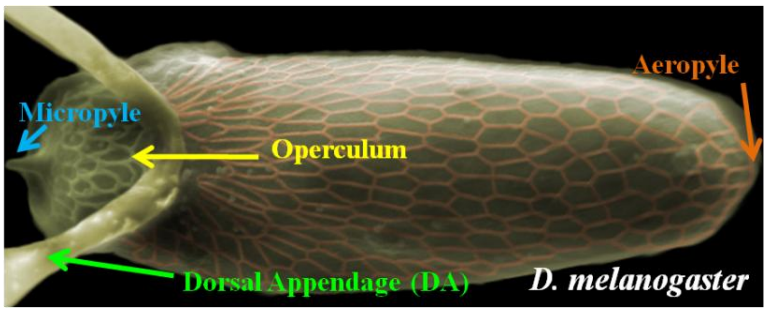

Figure 1: *Drosophila* eggshell structures. The *melanogaster* eggshell structures include Micropyle (blue) at the anterior end, Operculum (yellow), Dorsal Appendages (green), and Aeropyle (orange) at the posterior end.

The number, size, position, and shapes of DAs vary remarkably among *Drosophila* species (Fig. 2) (Hinton, 1981; Kagesawa et al., 2008; Niepielko et al., 2011). For example, *D. melanogaster* has 2DAs, *D. phalerata* has 3DAs, and *D. virilis* has 4DAs (Fig. 2 A, I, M). While the formation of DAs was extensively studied in *D. melanogaster*, the mechanisms underlying the formation of different DAs numbers is still unknown (Kagesawa et al., 2008).

Figure 2

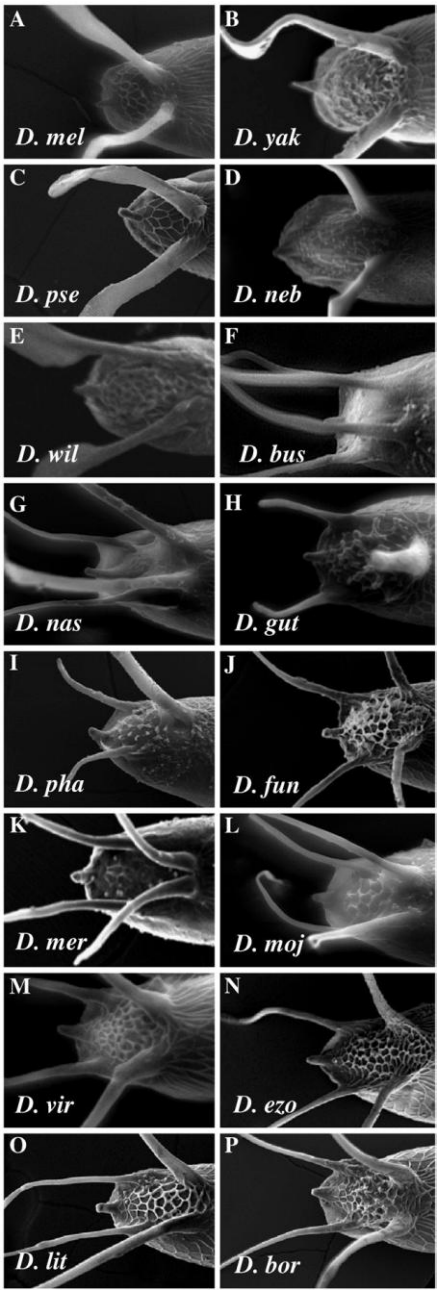

Figure 2: Varieties of eggshell morphologies in selected species from the genus *Drosophila.* (A–E) Subgenus *Sophophora*, represented by *D. melanogaster* (*D. mel*), *D. yakuba* (*D. yak*), *D. pseudoobscura* (*D. pse*), *D. nebulosa* (*D. neb*), and *D. willistoni* (*D. wil*), with two DAs eggshells. (F) Subgenus *Dorsilopha, D. busckii* (*D. bus*) has eggshell with four DAs. (G–P) Subgenus *Drosophila*, with three DAs eggshells *D. guttifera* (*D. gut*) and *D. phalerata* (*D. pha*) (H, I), and with four DAs eggshells *D. nasuta* (*D. nas*), *D. funebris* (*D. fun*), *D. mercatorum* (*D. mer*), *D. mojavensis* (*D. moj*), *D. virilis* (*D. vir*), *D. ezoana* (*D. ezo*), *D. littoralis* (*D. lit*), and *D. borealis* (*D. bor*) (G, J–P). All SEM micrographs show the anterior portion of the eggshells in dorsal views and anterior is to the left.

(Niepielko et al., 2011)

In Hawaiian *Drosophila*, a lumen-like eggshell structure has been structurally characterized. Known as the dorsal ridge (DR), this structure extends from the base of DAs towards the posterior aeropyle. It was suggested to function in gas exchange (Fig. 3) (Margaritis et al., 1983; Piano et al., 1997). This structure is absent from *D. melanogaster* eggshells (Fig. 1). Originally, it was believed to be exclusive to Hawaiian *Drosophila* (Margaritis et al., 1983; Piano et al., 1997). A detailed characterization of the DR was done in *D. grimshawi* (Margaritis et al., 1983; Margaritis et al., 1980; Piano et al., 1997); however, the signaling mechanism controlling DR formation is unknown.

Figure 3

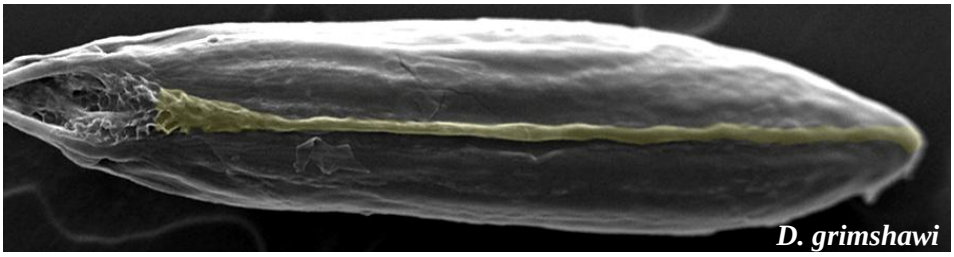

Figure 3: The dorsal ridge eggshell structure. The dorsal ridge (highlighted yellow) has been characterized in Hawaiian *Drosophila* such as *D. grimshawi*. The dorsal ridge (yellow) extends from the base of the DAs towards the posterior aeropyle.

1.2 Model system: *Drosophila* oogenesis

The formation of the *Drosophila* eggshell is an established model system for studying cell signaling and tissue patterning in epithelial cells (Berg, 2005). Oogenesis comprises 14 morphologically distinct stages (Fig. 4A) (Spradling, 1993). At mid oogenesis the egg chamber, which is the precurser to the mature egg, has three main compartments; the nurse cells (NCs), the oocyte, and the follicle cells (FCs) (Fig. 4B). The NCs are responsible for nourishing the developing oocyte with different RNAs and proteins. The largest compartment, the oocyte, becomes the developing embryo after fertilization. Surrounding the oocyte are the FCs (Fig. 4B), a monolayer of cells that

ultimately folds into the eggshell and its 3D structures (Fig. 1) (Cavaliere et al., 2008; Horne-Badovinac and Bilder, 2005; King, 1970).

Figure 4

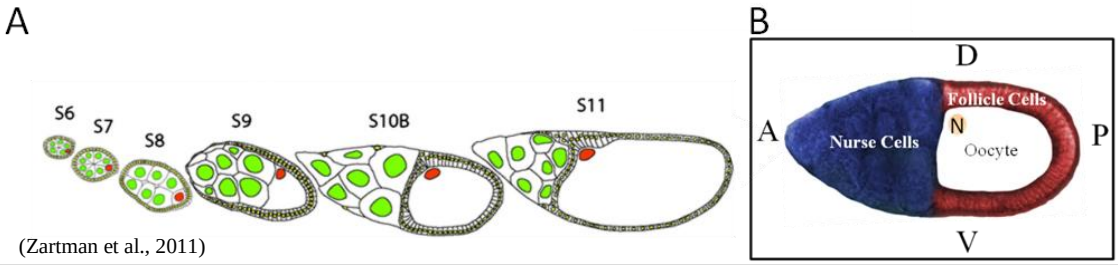

(Zartman et al., 2011)

Figure 4: Oogenesis in *Drosophila*. (A) An example of the morphologically defined stages an egg chamber undergoes during oogenesis. (B) A single egg chamber at stage 10b is shown with its defining features and orientation. At the most anterior region, "A", are the nurse cells (NCs) (blue). To the right of the NCs is the developing oocyte (white); the location of the oocyte's nucleus (N) (orange) defines dorsal, "D". Surrounding the oocyte is a two-dimensional tissue layer of follicle cells (FCs) (red).

1.3 Morphogen gradients

The folding of the 2D FCs into the 3D eggshell is followed by extensive tissue patterning that is guided by cell signaling. This raises the question, how do cells know their position in a tissue? Tissue differentiation is guided by the chemical environment sampled by the cells. These chemicals or morphogens, are distributed non-uniformly in the tissue. Morphogen gradients transform naïve cells into a patterned, non-uniform differentiated tissue (Turing, 1952; Wolpert, 1969). More specifically, a morphogen is secreted from a localized source and forms a gradient within a tissue; from high to low as it travels away from its source. Cells in the tissue respond by their position in the gradient by expressing different sets of genes (Fig. 5).

Figure 5

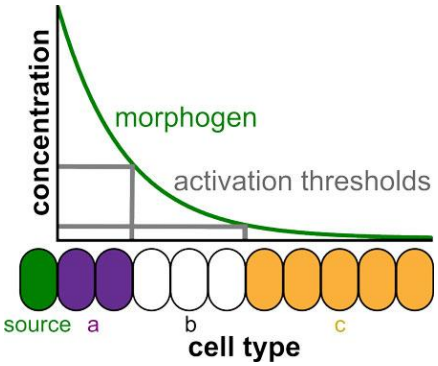

(Muller et al., 2013)

Figure 5: Morphogen gradients. A morphogen is secreted from a localized source (green cell) and creates a gradient that degrades farther away from the source. Morphogen gradients are interpreted by cells within a tissue causing non-uniform gene expression (shown with cell type a, b, and c).

1.4 Signaling pathways

Cell signaling pathways act in tissues in a morphogen response manner. Two main signaling pathways control patterning in the FCs. The morphogen, or ligand, Decapentaplegic is the homolog to the mammalian bone morphogentic protein (BMP) type 2, 4 and is part of the TGF-β super family of signaling molecules that activates BMP signaling pathway (Massague and Gomis, 2006; Parker et al., 2004). Additionally, activation of receptor tyrosine kinases (RTKs), such as the epidermal growth factor receptor (EGFR), also regulates many developmental processes (Sopko and Perrimon, 2013). Both signaling pathways are highly conserved and are vital mediators of tissue development across animals (Massague et al., 2000; Parker et al., 2004; Shilo, 2005). Irregular activations of BMP and of EGFR signaling are associated with various developmental diseases and cancers (Massague et al., 2000; Mitsudomi and Yatabe, 2010)

1.5 The bone morphogenetic protein pathway

Signaling through the BMP pathway begins when a ligand dimer binds to a complex of type I and type II BMP receptors, which in turn phosphorylates the intracellular signaling mediator R-SMAD (P-SMAD). Activated P-SMAD dimerizes and binds a co-SMAD and other proteins, which leads to the translocation of the complex into the nucleus, where it acts as a transcriptional regulator (Massague et al., 2000; Parker et al., 2004; Pyrowolakis et al., 2004; Wu and Hill, 2009) (Fig. 6A).

In the FCs of *D. melanogaster*, the DPP ligand, is secreted from a localized anterior source (Fig. 6B (Dequier et al., 2001; Dobens et al., 1997; Peri and Roth, 2000)), to form an anterior-posterior (A/P) gradient of DPP. The DPP receptor, *thickveins*

(*tkv*), is dynamically expressed. Initially, *tkv* is uniform throughout the FCs (Fig. 6C). Later, it is localized to two dorsolateral patches on either side of the dorsal midline (Fig. 6D (Mantrova et al., 1999; Yakoby et al., 2008b)). Consequently, DPP that signals through a uniformly expressed receptor generates an anterior signaling pattern along the oocyte and nurse cells border (Fig. 6E, F (Jekely and Rorth, 2003; Peri and Roth, 2000; Shravage et al., 2007)). Later, signaling becomes asymmetric along the dorsal-ventral (D/V) axis and appears in two dorsolateral patches on either side of the dorsal midline that corresponds to the late pattern of *tkv* (Fig. 6G (Lembong et al., 2009; Yakoby et al., 2008b)). Thus, in *D. melanogaster*, changes in *tkv* expression in the FCs control the dynamics of BMP signaling; initially, along the A/P axis, and later along the D/V axis as well.

Figure 6

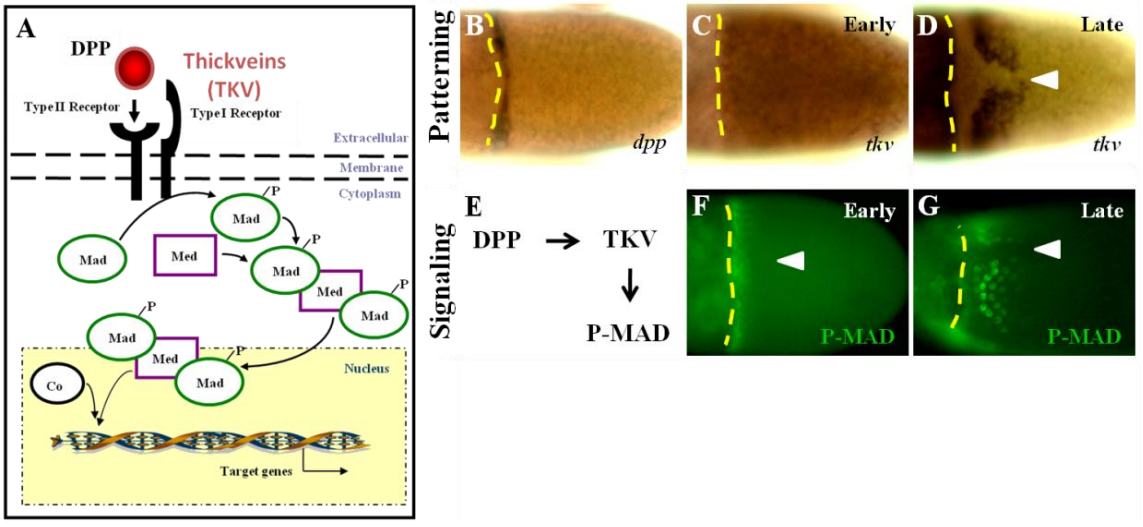

Figure 6: Dynamic expression of *tkv* guides BMP signaling. (A) A schematic representation of BMP signaling in the FCs. (B) The *dpp* ligand is expressed in anterior FCs. Broken yellow line denotes the anterior border of FCs over the oocyte. (C) Early *tkv* expression is uniform throughout the FCs. (D) Late *tkv* expression is repressed in the dorsal midline and is expressed in two dorsolateral patches on either side of the dorsal midline (white arrowhead marks the dorsal midline). (E) A Simple illustration of BMP signaling activation which can be monitored for an antibody against P-MAD. (F) Early BMP signaling (P-MAD, green) is restricted to the FCs along the anterior border. (G) Late BMP signaling appears as two dorsal patches on either side of the dorsal midline, similar to the late pattern of *tkv*. (D, F, and G) Dorsal views.

1.6 The epidermal growth factor receptor pathway

EGFR signaling plays a critical role during oogenesis. Activation of the EGFR pathway begins when the TGF-α-like signaling molecule GRK, is secreted from the oocyte and binds to the EGFR; activating a series of phosphorylation events via the RAS-RAF-MAPK pathway in the FCs; which in turn creates a dorsal/ventral EGFR activation gradient (Neuman-Silberberg and Schupbach, 1993, 1994; Sapir et al., 1998; Shilo, 2005) (Fig. 7A-D). In the egg chamber, Gurken's RNA *(grk*) is localized near the oocyte's nucleus where it translates into GRK protein. Initially, the nucleus is localized at the posterior end of the egg chamber and later migrates asymmetrically to the cortex of the oocyte (Fig. 7E). This process first determines the anterior-posterior (AP) followed by setting the dorsal-ventral (DV) axes of the egg (Fig. 7). Loss of GRK led to eggshells with no AP or DV axes (Berg, 2005; Neuman-Silberberg and Schupbach, 1996; Ray and Schupbach, 1996; Van Buskirk and Schupbach, 1999).

Figure 7

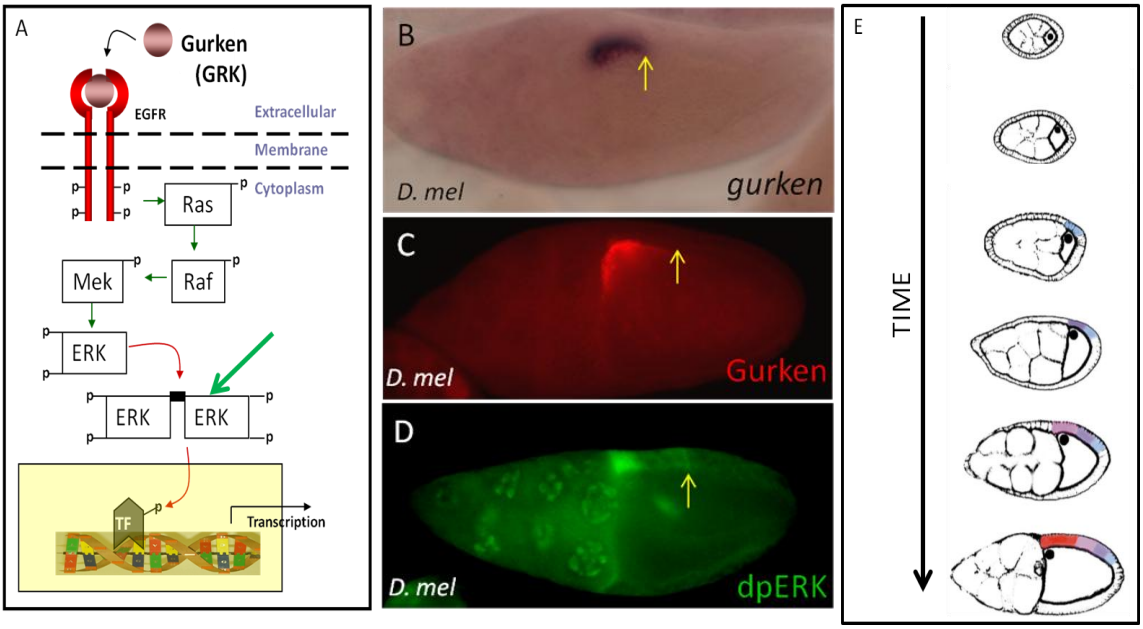

(Van Buskirk and Schupbach, 1999)

Figure 7: Gurken signals through the EGFR during *Drosophila* oogenesis. (A) Schematic representation of EGFR signaling in the FCs. (B) Gurken RNA (*grk)* and its protein (GRK) (C) are localized near the oocyte nucleus. (D) This localization causes EGFR activation in the follicle cells directly above the nucleus; monitored by an antibody against dpERK (green arrow in A). (E) The oocyte nucleus in early eggs chambers is located at the posterior end of the oocyte and later migrates towards the anterior and is maintained in a dorsal anterior position throughout later stages of oogenesis. In all images, anterior is to the left and the yellow arrow points to the most posterior detection of *grk*/GRK/dpERK.

1. 7 Follicle cell patterning

Eggshell morphogenesis precedes an extensive patterning of the FCs. A recent study surveyed the expression patterns of 81 genes over four developmental times and found 36 unique patterns that ranged in complexity (Yakoby et al., 2008a). An example of the unique patterns observed during oogenesis is seen in figure 8. To analyze patterning dynamics and complexity, expression patterns were broken into six basic building blocks, or primitives, that represent the shapes of specific domains (Fig. 8B (Yakoby et al., 2008a)). The primitives include midline (M), dorsal (D), anterior (A), roof (R), floor (F), and uniform (U). Midline denotes a region of high levels of EGFR signaling, dorsal represents a region with intermediate levels of EGFR signaling, anterior is mark the region set by high levels of early BMP signaling, roof is the region that will become the future top of the dorsal appendages, floor is the domain that represents the future bottom of the dorsal appendages, and uniform represents expression throughout the FCs (Yakoby et al., 2008a). Simple building blocks were combined using various operations; intersection (∩), difference (\), union (∪), and addition (+) to create the more complex patterns (Fig. 8 and (Yakoby et al., 2008a)). Examples of using the operations and primitives to construct more complex patterns is presented in figure 8C. Analysis of eggshell patterning found that most genes are highly dynamic. Specifically, there is a

74% probability that the expression pattern of a gene will be different at another developmental time. In addition, new patterns that appeared in later stages were more likely to be complex patterns, than earlier simple shapes (Yakoby et al., 2008a).

Figure 8

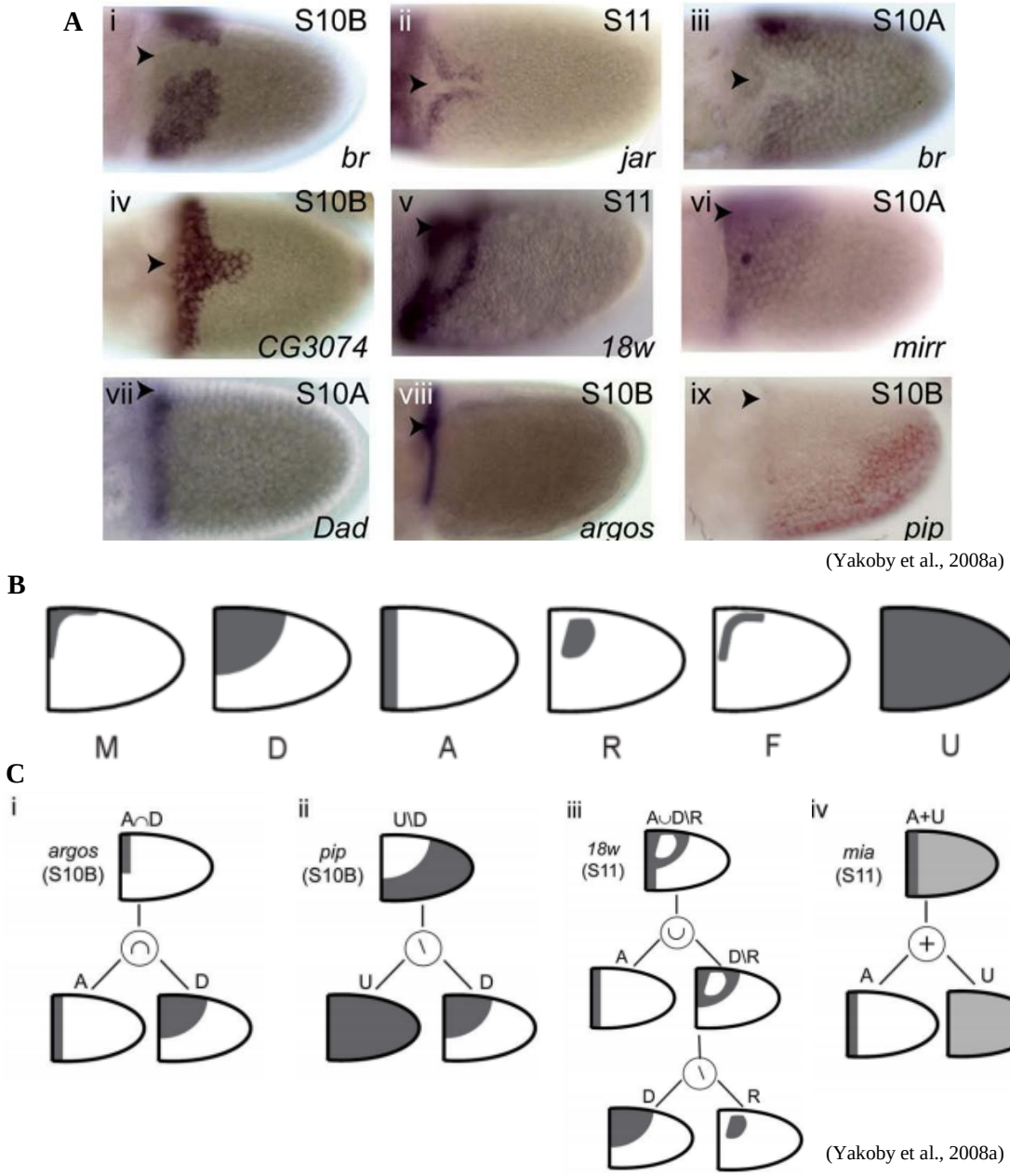

Figure 8: Examples of expression patterns in the FCs and combinatorial code. (A) Gene expression patterns vary in complexity at various stages. (B) The basic primitives used to construct more complex patterns. Midline (M), Dorsal (D), Anterior (A), Roof (R), Floor (F), and Uniform (U). (C) Construction of complex patterns using the primitives and operations: intersection (∩), difference (\), union (∪), and addition (+). Black arrowhead points to the dorsal midline, egg chamber stages are in the top right, the gene name is on the bottom right and anterior is to the left.

1.8 Cell signaling and morphological diversity

Variations across species have been associated, to a large extent, with modifications in the distribution of signaling pathway outputs (Ashe and Briscoe, 2006; Carroll, 2005, 2008; Davidson and Erwin, 2006; De Robertis, 2008; Parchem et al., 2007). Each signaling pathway comprises multiple components; therefore, identifying the molecules responsible for signal diversification is a key requirement to discovering the underlying mechanisms governing tissue evolution. For instance, the diversity in beak morphology in Darwin's Finches has been associated with expression levels of the BMP4 ligand, the vertebrate homolog of BMP-like ligand DPP in *D. melanogaster* (Abzhanov et al., 2004). In *D. melanogaster*, formation of the amnioserosa, an extra embryonic tissue produced by the dorsal ectoderm, is regulated by BMP signaling (Ashe and Levine, 1999; Eldar et al., 2002). Interestingly, in the mosquito *Anopheles gambiae*, the dorsal ectoderm expands into two separate tissues, the amnion and serosa. In this case, the reduced levels of the negative BMP regulator Short-gastrulation (Sog) accounts for the expansion of BMP signaling and for the broadening of the dorsal ectoderm domain along the DV axis (Goltsev et al., 2007).

In *Drosophila* species with different number of DAs, the Matsuno lab found a correlation between the number of EGFR signaling domains and number of future DAs; however the mechanism controlling EGFR signaling domains is still unknown (Kagesawa et al., 2008). We found that BMP signaling is dynamic and diverse in the FCs of *Drosophila* species with different DA morphologies and that these signaling differences are correlated to changes in the spatial expression of *tkv* (Niepielko et al., 2011). Here, we used computational modeling to simulate changes in BMP signaling and

found that quantitative changes in *tkv* expression also affect BMP signaling outputs in species with different DA morphologies.

In addition to DAs morphology, eggshells from different species also have diverse dorsal ridge (DR) morphologies. Using gene patterning and domain association, we predicted that the DR domain is regulated by EGFR signaling. Specifically, patterns in the DR domain clustered with EGFR regulated domains. Based on this prediction, we focused on EGFR signaling and DR formation. We found that DR morphologies correlate with EGFR signaling and GRK protein patterns in the DR domain. In the DR species *D. willistoni*, we successfully genetically perturbed EGFR signaling and dorsal ridge formation by perturbing GRK. Expression of *D. willistoni* GRK (*w*GRK) in *D. melanogaster* rescues a *grk* null *D. melanogaster* phenotype and in some cases, *w*GRK is sufficient to produce a dorsal ridge-like structure on *D. melanogaster* eggshells. Our results support the idea that changes in major components, including receptors and ligands, underlie the evolution of morphologies.

Results

Chapter 2: Evolution of BMP signaling in *Drosophila* oogenesis: a receptor-based mechanism

2.1 Developmental and evolutionary dynamics of BMP signaling in follicle cells

Patterning related to DAs formation has been extensively studied (Berg, 2005). Specifically, in *D. melanogaster*, DAs are formed by two non-overlapping groups of cells. One group is marked by the zinc-finger transcription factor Broad (BR), expressed in two dorsolateral patches on both sides of the dorsal midline (Deng and Bownes, 1997). These cells will form the top or roof of each DA (Ward and Berg, 2005) (Fig. 9). The other group is marked by a protease in the EGFR pathway, rhomboid, which is expressed in the cells adjacent to the BR domain (Ruohola-Baker et al., 1993). These cells will form the bottom, or floor, of each DA (Dorman et al., 2004; Osterfield et al., 2013) (Fig. 9).

Figure 9

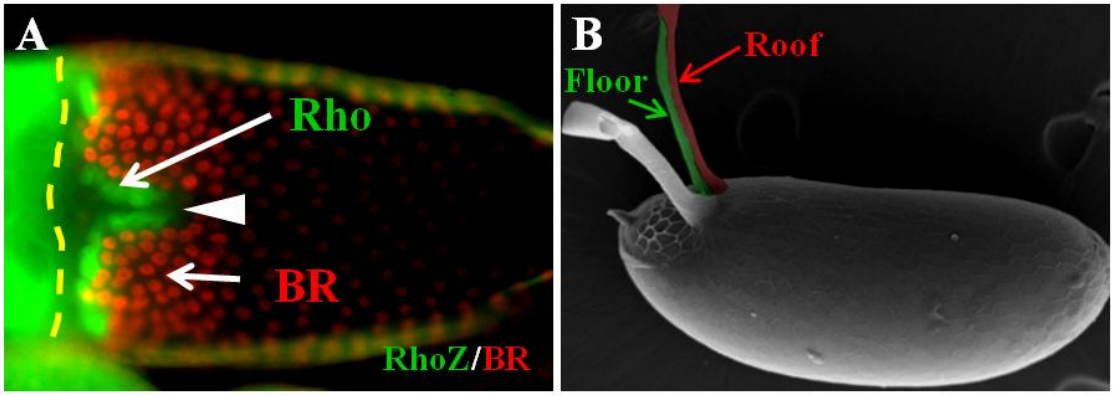

Figure 9: Dorsal appendage patterning in the FCs. (A) Expression pattern of a LacZ reporter for rhombiod (RhoZ, green). The RhoZ is adjacent to the BR (red)-expressing domains on both sides of the dorsal midline (arrowhead). (B) Scanning electron microscope image of a *D. melanogaster* eggshell. One of the two DAs is artificially colored to mark the floor (green) and roof (red) domains of the appendage (A is dorsal view and B is a lateral view, anterior is to the left in both images, broken yellow line denotes anterior region).

We previously established that, similar to *D. melanogaster* (Fig. 6), BMP signaling is dynamic in the FCs of multiple *Drosophila* species (Niepielko et al., 2011; Yakoby et al., 2008b). In addition, the patterns of BMP signaling are spatially different among the species. The signaling patterns were determined based on the spatial distribution of the phosphorylated form of the intracellular signal transducer Mothers against Dpp (P-MAD). To characterize the spatial patterns of P-MAD, we used Broad to mark the roof domain of the DA forming cells (Fig. 9). We were particularly interested in the overlap between the pattern of BMP signaling, assayed by P-MAD, and the roof domain.

Previously, the patterns of P-MAD in the FCs of ten *Drosophila* species were clustered into three unique spatially distinct patterning groups (Niepielko et al., 2011). In reference to the BR (roof) domain, the pattern of P-MAD either overlapped the roof domain, or overlapped the roof and floor domains, or was completely absent from the roof and floor domains (Niepielko et al., 2011). Interestingly, these patterning groups clustered according to their species' phylogenetic associations. This classification implies that spatial patterns of BMP signaling can be predicted based on phylogeny.

To test this prediction, we selected three new *Drosophila* species, which were predicted to represent each of the three patterning groups. The early pattern of P-MAD in the three species is restricted to the FCs overlying the border between the oocyte and the nurse cells (Fig. 10A-C), which is in agreement with the pattern found in other species (Niepielko et al., 2011; Yakoby et al., 2008b). *D. erecta* was selected to represent the *melanogaster* sub-group. In this group, the pattern of P-MAD fully overlaps the roof cells (Niepielko et al., 2011; Yakoby et al., 2008b), which is the case for *D. erecta* (Fig. 10D-

D''). The second patterning group comprises species such as *D. nebulosa* and *D. willistoni* from the *willistoni* sub-group (Niepielko et al., 2011). We selected *D. tropicalis* to represent this group (O'Grady and Kidwell, 2002). As expected, in addition to overlapping the roof domain, P-MAD is found in the adjacent floor domain (Fig. 10E-E''). The third patterning group comprises species from the *guttifera* and *quinaria* groups including *D. guttifera* and *D. phalerata*, respectively (Niepielko et al., 2011). We selected *D. quinaria* to represent this group. Like the other two species in this group, P-MAD is absent from the roof and floor domains, and it appears as an anterior stripe that is repressed on its dorsal side (Fig. 10F-G'). In summary, as predicted by phylogenetic associations (Niepielko et al., 2011), spatial distributions of P-MAD in the three selected species reflect their corresponding patterning groups.

Figure 10

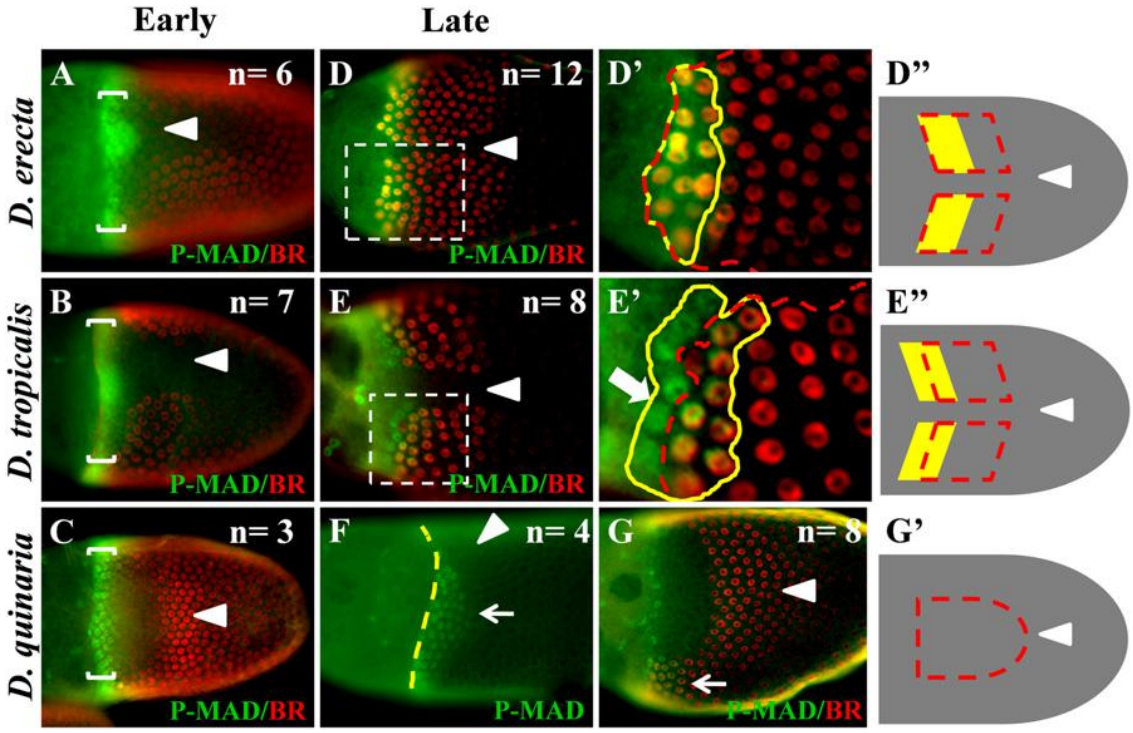

Figure 10: Activation patterns of BMP signaling differ across *Drosophila* species. (A–C) Early BMP signaling (P-MAD, green) in *D. erecta*, *D. tropicalis*, and *D. quinaria* appears as an anterior band of 2–3 cell rows (white brackets) along the anterior border of the FCs. White arrowhead denotes the dorsal midline. BR (red) marks the future roof cells of the DAs. We focus on the overlapping between BR (red broken line) and P-MAD (yellow line) patterning domains to distinguish among the types of BMP signaling patterns. (D–F) Late patterns of BMP signaling differ across species. (D, D', and D'') Late BMP signaling in *D. erecta* has two dorsolateral patches on either side of the dorsal midline that overlap the BR domains. White broken lined box in D marks the inset in D'. (D'') A schematic representation of late BMP signaling in *D. erecta* (the red broken line represents the BR domain, and the yellow box represents BMP signaling). (E, E', and E'') Late BMP signaling in *D. tropicalis* appears as two dorsolateral patches on both sides of the dorsal midline. Signaling overlaps the BR domain and also a row of cells adjacent to the BR cells, the floor domain. White box marks the inset region in E'. The white arrow points to the additional region of BMP signaling in E'. E'' is a schematic representation of late BMP signaling found in *D. tropicalis*. (F) Late BMP signaling in *D. quinaria* is absent from the dorsal BR domain (lateral view of P-MAD). (G) Dorsal view of the absence of BMP signaling from the future middle appendage. (G') A schematic representation of the BMP signaling pattern found in *D. quinaria*. Images are dorsal views, and anterior is to the left. Numbers (n) represent the egg chambers' counts seen for each phenotype. Arrowhead denotes the dorsal midline. The anterior domains of signaling are not represented in the schematics.

species correlate with spatial distributions of *tkv* (Niepielko et al., 2011; Yakoby et al., 2008b). The early pattern of *tkv* is uniform throughout the FCs of the three selected species (Fig. 11A-C). Later during egg development, *tkv* becomes patterned. In *D. erecta*, *tkv* is expressed in two dorsolateral patches on both sides of the dorsal midline (Fig. 11D-D'). In *D. tropicalis*, *tkv* is expressed in two dorsolateral patches that reflect the distance between the two corresponding dorsolateral patches of P-MAD in this fly (Figs. 11E, 11E, E'). This was determined by comparing the number of cells between the BR domains to the number of cells between the *tkv* domains (Niepielko et al., 2011). In *D. quinaria*, *tkv* is expressed in an anterior domain and is repressed on the dorsal side (Fig. 11F, F'). Consistent with our previous findings, the patterns of *tkv* in the selected species are consistent with the corresponding spatial patterns of BMP signaling in these species (Fig. 10).

Figure 11

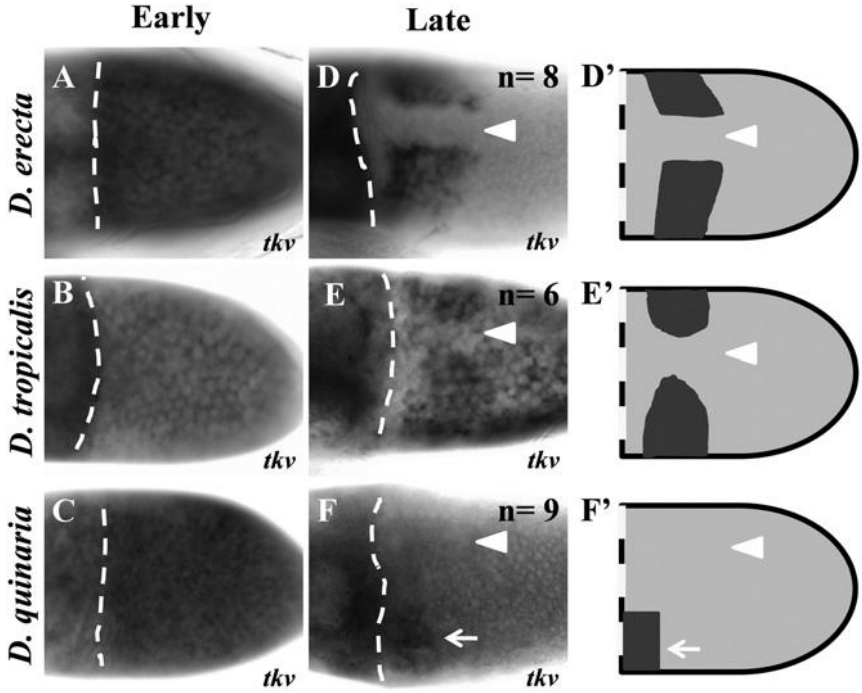

Figure 11: Expression patterns of *tkv* differ across *Drosophila* species. (A–C) Early *tkv* in *D. erecta*, *D. tropicalis*, and *D. quinaria* is uniformly expressed throughout the FCs (white broken line marks the anterior border of FCs). (D and E) Dorsal views of late *tkv* patterns in *D. erecta* and *D. tropicalis* that appear in two dorsolateral patches on either side of the dorsal midline (white arrowhead marks the dorsal midline). (F) The late pattern of *tkv* in *D. quinaria* appears in an anterior band that is repressed in its dorsal domain (white arrow). (D'–F') Schematic representations of late patterns of *tkv*. (D,E) Images are dorsal and (F–F') lateral views. In all images. anterior is to the left. Numbers (n) represent the egg chambers' counts seen for each phenotype.

2.2 Computational modeling of dynamics and diversity of BMP signaling

The patterns of BMP signaling vary among *Drosophila* species in two ways. First, BMP signaling can overlap the roof domain, or the roof and floor domains, or be completely absent from these domains. Second, within each spatial pattern, the width of the signaling domain is different. For example, in *D. erecta*, the P-MAD domain spans ~2 cell-rows that overlaps the roof cells; whereas, in *D. tropicalis*, in addition to partially overlapping the roof cells, P-MAD is also present in the floor cells, totaling ~3 cell-rows (Fig. 10D', E'). As a first step towards studying this diversity, we used a biophysical

model to study how changes in the pattern and level of *tkv* expression affect the spatial pattern of BMP signaling.

The model is based on the steady-state solution of differential equations on the surface of an ellipsoid (Goentoro et al., 2006; Lembong et al., 2008). The model considers a constant flux of DPP from the stretch-cells oocyte boundary (Dequier et al., 2001; Peri and Roth, 2000; Twombly et al., 1996), and it assumes that a single receptor pattern regulates the pattern of P-MAD activation after the internalization of the ligand-receptor complex. Ligand degradation depends on a receptor after the internalization (Mantrova et al., 1999; Yakoby et al., 2008b). The model requires two inputs - the spatial profile of the receptor expression and the length scale of DPP diffusion (φ). The φ value provides the ratio between the tissue size (L) and the length scale diffusion of the ligand (λ) (Lembong et al., 2008; Reeves et al., 2006).

$$\varphi^2 = \left(L/\lambda\right)^2 \quad where, \quad \lambda \propto 1/\sqrt{R}$$

The parameter φ is a dimensionless measure of the extent to which the ligand diffuses in the FCs through a field of a receptor. Note that λ is inversely related to the receptor level (R). Thus, an increase in the level of the receptor expression would lead to a decrease in λ and an increase in φ. Thus, increasing the receptor would lead to the sharpening of the P-MAD gradient towards the source of the ligand. The complete model is published elsewhere (Goentoro et al., 2006; Lembong et al., 2008).

Considering the domains of BMP signaling in each species and the width of the signaling in each domain, we adjusted the receptor distributions and the φ values for each signaling group (Fig. 12). Using this model, we simulated signaling in four types of receptor distributions. A uniform receptor distribution represents the early pattern of *tkv*

in all patterning groups (Fig. 12A). The next two groups represent the late patterns of *tkv*, in which, the receptor is in two dorsolateral patches (Fig. 12B, C). The gap between the two dorsolateral domains of the receptors in Fig. 12B is greater than the gap in Fig. 12C; this difference reflects the patterns of *tkv* in *D. erecta* and *D. tropicalis*, respectively (Fig. 11D, E). In the last group, the receptor is patterned only in an anterior stripe that is repressed on the dorsal side (Fig. 12D), which represents the pattern of *tkv* in *D. quinaria* (Fig. 11F).

We reasoned that an increase in the φ value will decrease the diffusion length of the ligand over a field of receptors, which will generate progressively restricted signaling patterns in domains facing the ligand source. Previously, the pattern of BMP signaling in *D. melanogaster* was simulated with the φ of 20 (Lembong et al., 2008). This value takes into consideration a length of ~25 FCs from the anterior end of the oocyte to the posterior end. The value corresponds to the ligand diffusion length of 1-2 cell-widths before DPP is captured and degraded after internalization. Based on the pattern of early signaling that spans ~3 cells wide (Fig. 10A-C), we selected φ = 15 to simulate this pattern (Fig. 12E). We used values of 20 and 15 to represent the ~2 and ~3 cells wide P-MAD domains that correspond to the late patterns of signaling in *D. erecta* and *D. tropicalis*, respectively (Fig. 12F, G). The wider domain of signaling in *D. quinaria* was simulated with the value of 10 (Fig. 12H); reflecting ~5 cells wide domain of lateral signaling (Fig. 10F). In summary, using this model, we demonstrate that by changing the spatial distribution of the receptor and diffusion properties of the ligand, we can simulate the spatial patterning of BMP signaling in the three patterning groups.

Figure 12

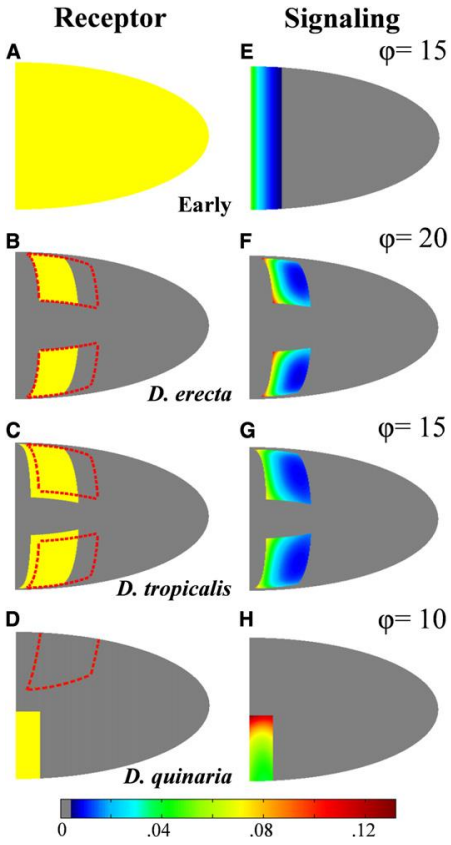

Figure 12: Two-dimensional model of BMP signaling dynamics and diversity solved on a prolate spheroidal grid. The model is based on an anterior secretion of DPP that activates signaling in the FCs by binding to TKV. The distributions of TKV are based on the types of *tkv* expression patterns (Fig. 11). (A) For all species, early *tkv* (yellow) is uniform throughout the FCs. (B–D) Different patterns of *tkv* simulate the observed patterns found in *D. erecta*, *D. tropicalis*, and *D. quinaria*, which are based on in situ hybridizations (Fig. 11). Red broken line marks the BR domain. (E–H) Simulations are based on the patterns of BMP signaling across species (Fig. 10) and the spatial distributions of *tkv* (Fig. 11). (E) BMP signaling simulation using a uniform receptor pattern restricts signaling to the anterior domain. (F and G) Signaling simulations of D. *erecta* and D. *tropicalis*, respectively (dorsal view). (H) Signaling simulation in *D. quinaria* in the absence of a dorsal *tkv* (lateral view). The values of φ were adjusted to reflect the experimentally observed changes in signaling activation domains of ~2, 3, and 5 cells wide (Fig. 10).

2.3 The levels and distributions of *tkv* determine the shapes of BMP signaling gradients

The model takes into consideration that the spatial distribution of TKV expression determines the pattern of signaling (Lembong et al., 2008). Previously, we demonstrated by genetic perturbations in *D. melanogaster* that qualitative changes in the patterns of *tkv* are consistent with the consequent spatial distributions of BMP signaling (Niepielko et al., 2011). Thus, *tkv* is sufficient to determine the spatial distribution of signaling, which may account for the diverse patterns of BMP signaling across species (Figs. 10, 11). However, each signaling pattern across species is shaped differently. For example, the late patterns of P-MAD in *D. erecta*, *D. tropicalis*, and *D. quinaria* consist of 2, 3, and 5

cells long domains, respectively (Fig. 10D-F). Thus, we aim to explore whether quantitative changes in TKV are sufficient to modify the shapes of BMP signaling domains.

In the model, the values of φ depend on the expression levels of the receptor (Lembong et al., 2008). Consequently, higher φ values reflect higher receptor levels. For higher values of φ, signaling increases in proximal domains to the ligand source and decreases in more distal domains (Fig. 13A). This predicts that changes in the levels of the *tkv* receptor will restrict the BMP signal to a domain closer to the anterior end. As predicted by the model, higher values of φ (10, 15, and 20) have lower λ values (12.3, 8.2, and 6.15), respectively. To test these predictions, we took advantage of the transition developmental stage between a uniform and a patterned *tkv* expression (Yakoby et al., 2008b). This stage is characterized by the initial symmetry breaking of BMP signaling along the DV axis. Specifically, at stage 10B, the pattern of P-MAD is ~5 cells wide on the dorsal side and ~2 cells wide on the dorsolateral and ventral sides (Fig. 13B (Yakoby et al., 2008b)).

Previously, we suggested that during the transition from a uniform to a patterned receptor, the repression of *tkv* in the dorsal midline lowers the levels of TKV (Yakoby et al., 2008b). This, in turn, enables DPP to travel through the midline and transform the anteriorly restricted signal to a wide signaling domain (Figs. 13B). To test this mechanism directly, we employed two GAL4 drivers to weakly and highly increase the levels of *tkv* in the FCs at this developmental stage. Given the anterior source of DPP, we expected that a gradual increase in *tkv* will progressively restrict signaling to anterior cells. Using the 55B-GAL4 and CY2-GAL4 drivers (Queenan et al., 1997), we weakly

and strongly expressed *tkv* in the FCs. Increasing the levels of receptor was sufficient to gradually restrict P-MAD to the anterior domain (Fig. 13C, D). Plotting the intensities of P-MAD gradients, we found that by increasing the levels of *tkv*, we could successfully lower the λ values and increase the φ value (Fig. 13E). Specifically, obtained from the fitted curves to the intensity plots of BMP signaling (see M&M), we found lower λvalues (16.3, 11.4, and 8.1) and higher φ values (7.6, 10.8, and 15.1), respectively, for the gradual increase in the levels of TKV. In summary, as predicted by the model, quantitative changes in *tkv* levels regulate the distributions of BMP signaling domains.

Figure 13

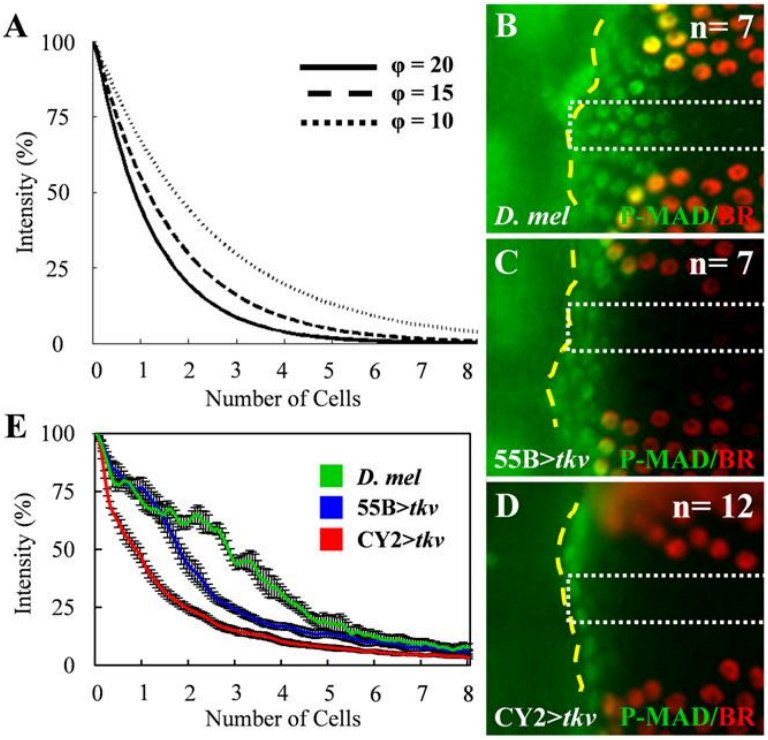

Figure 13: Levels of *tkv* expression control the gradient of BMP signaling. (A) Signaling distribution computed for different values of φ over a field of a uniform receptor. The model predicts that by increasing the φ-values, the activation gradients of P-MAD will become sharper. (B–D) Changes in the pattern of P-MAD due to modification in the levels of *tkv* expression during stage 10B of oogenesis (yellow broken line denotes the anterior domain). (B) In WT *D. melanogaster* (*D. mel*), BMP signaling appears in a 5–6 cell-wide domain (white box). (C) A weak increase in *tkv* expression, by using the 55B-GAL4 driver, restricts P-MAD to a 2–3 cell-wide domain (white box). (D) A strong increase in *tkv* expression, by using the CY2-GAL4 driver, restricts P-MAD to a 1–2 cell-wide domain. (E) Plot profiles of P-MAD in the dorsal midline of three different levels of *tkv* during mid-oogenesis. Gradients of P-MAD were measured in regions similar to the domains marked by the white dotted boxes in B–D. Each plot profile is an average of seven independent measurements (n= 7). The differences among the plots are statistically significant ($p < 0.01$). Standard errors are included on the curves. Dorsal view images and anterior is to the left.

Using the mathematical model, we examined the distribution of free ligand and signaling with and without dorsolateral receptor pattering (Fig. 14A-F). In the absence of dorsolateral receptor patterning, the free ligand reaches posterior and lateral domains, most likely due to the removal of a strong sink for DPP (Fig. 14A-F). As a result, the model predicts higher signaling levels in the lateral portion of the receptor's anterior domain due to the "spill over" of an anteriorly secreted ligand over the receptor's domain (Fig. 14D-F). Interestingly, in *D. quinaria*, a species in which *tkv* is naturally absent from the dorsal side, the domain of BMP signaling activation is considerably wider in this region (Fig. 10F). This observation is further supported by the higher levels and wider signaling in the lateral portion of the anterior domain after the removal of *tkv* from the dorsal domain in the FCs of *D. melanogaster* (Fig. 14G, G'). We note that this observation was previously missed (Niepielko et al., 2011), and the motivation to re-examine this perturbation came out of the simulations (Fig. 14F) (Niepielko et al., 2012).

2.4 Divergence of *tkv* pattern regulation

Previously, we used *tkv* sequences from 16 *Drosophila* species to determine the phylogenetic associations among them (Niepielko et al., 2011). Interestingly, these sequences were sufficient to build a phylogenetic tree that clustered the known groups in the genus *Drosophila.* Using a similar approach, we included the analysis of *tkv* sequences from *D. erecta*, *D. tropicalis*, and *D. quinaria*. As expected, *D. erecta* and *D. quinaria* clustered into their groups, the *melanogaster* subgroup and the *quinaria* group, respectively (Fig. 14H). *D. tropicalis* belongs to the *willistoni* sub-group (O'Grady and Kidwell, 2002), however, based on its *tkv* sequence, it was clustered into the *melanogaster* sub-group (Fig. 14H). This could indicate that *D. tropicalis* is closer to an

ancestral species that marks the loss of *tkv* in the floor domain in the *melanogaster* sub-group. In contrary, the ancestral fly could have gained the floor domain as seen in the *willistoni* sub-group (Niepielko et al., 2011). This type of analysis may indicate that the divergence of *tkv* is slower than that of other nuclear (alchohol dehydrogenase, and 28S ribosomal RNA) and mitochondrial (cytochrome oxidase II) genes, traditionally used to evaluate species divergence (O'Grady and Kidwell, 2002).

Figure 14

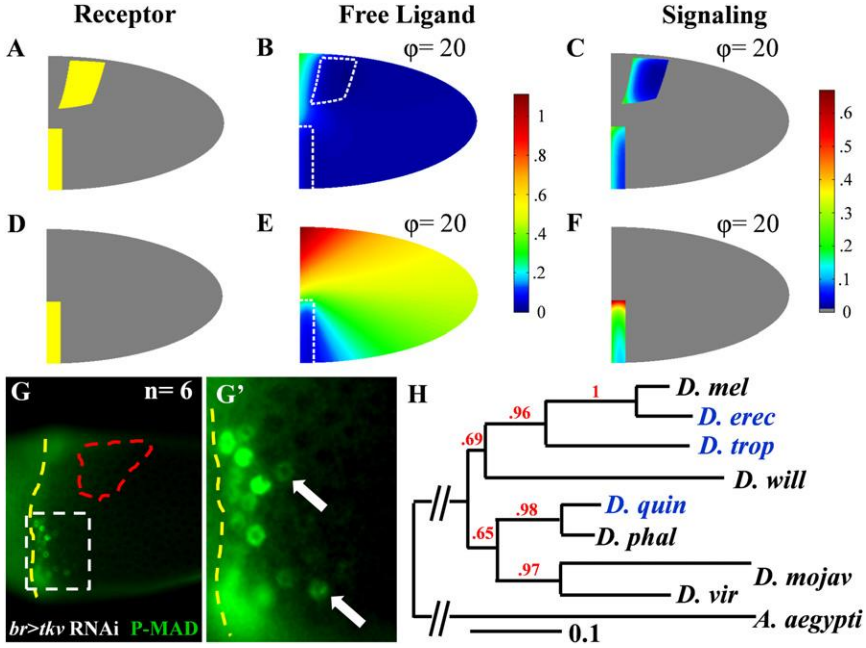

Figure 14: Simulations of free ligand and signaling distributions in different patterns of a receptor. Considering the anterior source of DPP diffusion, and (A) the late patterns of the receptor (*tkv*), (B) the levels of free DPP are high in the dorsal midline. (C) Signaling reflects the receptor's domains. (D) Removing the dorsolateral domain of the receptor, (E) increases tremendously the levels of free ligand, DPP, in the dorsal and lateral domains, (F) leading to an increased level of signaling on the dorsal portion of the patterned anterior receptor. These simulations reflect the pattern of P-MAD in *D. melanogaster*; thus, we selected the value of φ=20. (G) Depletion of *tkv* from the dorsolateral patches (br>tkvRNAi) was sufficient to eliminate P-MAD from these domains (lateral view; one domain is marked by a red broken line). (G') An inset (marked by a white broken line box) of G; arrows are pointing to the increased levels of P-MAD. Yellow broken line denotes the anterior border of the oocyte. (H) Phylogenetic analysis of eight *Drosophila* species that is based on the sequences of *tkv*. Previously analyzed species are in black (*D. mel, D. melanogaster; D. will, D. willistoni; D. phal, D. phalerta; D. mojav, D. mojavensis; and D. vir, D. virilis*) and the new species are in blue (*D. erec, D. erecta; D. trop, D. tropicalis*; and *D. quin, D. quinaria*). The tree is rooted by the corresponding *tkv* sequence of yellow fever mosquito *Aedes aegypti*. The scale bar represents the number of substitutions per site and is proportional to the estimated evolutionary divergence. Numbers shown on the tree are maximum-likelihood ratio values of the branches.

2.5 Depletion of the late pattern of *tkv* deforms DAs morphology

Perturbations in BMP signaling were associated with deformations in operculum size and in the number of DAs (Chen and Schupbach, 2006; Dequier et al., 2001; Dobens and Raftery, 2000; Peri and Roth, 2000; Shravage et al., 2007; Twombly et al., 1996; Yakoby et al., 2008b). These perturbations affected early stages of BMP signaling. Here, we investigate the role of late BMP signaling in eggshell morphogenesis by depleting *tkv* in the BR-expressing cells. Less than 10% of the eggshells appeared wild type and over 90% were deformed and appeared as short DAs or short and laid flat on the operculum (Fig. 15A, B). P-MAD was abolished on the dorsolateral patches of all egg chambers at stage 11 (Fig. 15C, C'). We could not notice any changes in early BR expression (Niepielko et al., 2011).

Figure 15

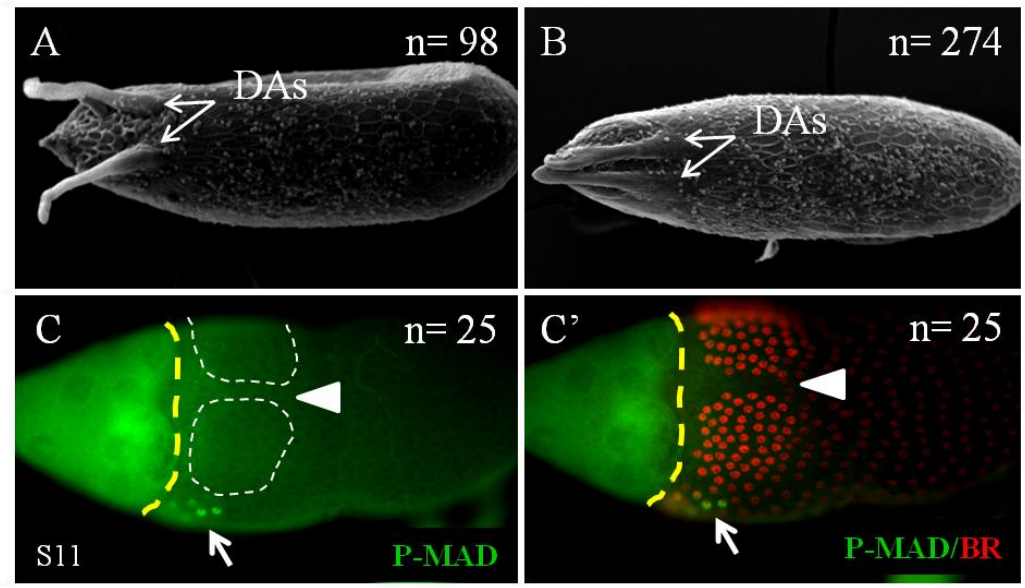

Figure 15: Late BMP signaling phase is involved in DAs morphogenesis. (A, B) SEM micrographs of eggshell from flies with depleted *tkv* on the BR domains. (C) Depletion of *tkv* by expressing *tkv* RNAi on the BR domain abolished the dorsolateral pattern of P-MAD on both sides of the dorsal midline (white broken lines denoted the BR domains). (C') Overlay of P-MAD and BR. The pattern of BR remained intact. White arrowhead denoted dorsal-midline, white arrow points to lateral BMP signaling, Dorsal-appendages (DAs).

Results

Chapter 3: Chorion Patterning: A window into gene regulation

3.1 Chorion patterning is dynamic and reflects eggshell morphologies

The dorsal ridge is a lumen-like structure along the dorsal most side of eggshells from *D. willistoni* and *D. nebulosa*; two species in the subgenus *Sophophora* (Niepielko et al., 2014). This structure is absent from *D. melanogaster* eggshells (Fig. 16A-C). The dorsal ridge was reported and characterized structurally only in eggshells from species of Hawaiian *Drosophila* (Fig. 3 and (Margaritis et al., 1983; Piano et al., 1997)). We assume that different structures reflect changes in follicle cell patterning among species. In addition, we aimed to determine whether tissue patterning can be used to study the signaling mechanism underlying dorsal ridge formation.

We selected one family of genes that participate in eggshell formation, the *Chorion protein* (*Cp*) genes (Fakhouri et al., 2006; Waring, 2000). This family includes nine genes: *Cp7fa*, *Cp7fb*, *Cp7fc*, *Cp15*, *Cp16*, *Cp18*, *Cp19*, *Cp36*, and *Cp38* (Griffin-Shea et al., 1982; Parks et al., 1986; Spradling, 1981). We focused on four developmental stages of oogenesis: S10A, S10B, S11, and S12 (Spradling, 1993) across three *Drosophila* species. In *D. melanogaster*, the expression patterns of seven of the nine *Cp* genes (excluding *Cp7fa* and *Cp19*), were published with different levels of spatial resolution (Griffin-Shea et al., 1982; Parks et al., 1986; Yakoby et al., 2008a). Our results are consistent with the known patterns in *D. melanogaster* and include a complete collection of all genes across three species (Fig. S1A-S1I).

We found that *Cp* genes are expressed dynamically and in different domains of the follicle cells of *Drosophila* species (Fig. 16D–L and supplementary Fig. S1A-S1I). Interestingly, in *D. willistoni* and *D. nebulosa*, we observe gene patterning that highly

correlates with the DR morphologies, reflecting the shorter DR in *D. willistoni* than *D. nebulosa* (Fig. 16B and C). Specifically, Cp genes that are patterned in the future DR domain of *D. willistoni* including *Cp7fa, Cp16,* and *Cp19* are shorter in length when compared with the corresponding patterns in *D. nebulosa* (Fig. 16K and L and supplementary Fig. S1A, S1E, and S1G). The same correlation was observed in the repression domain of *Cp7fc* in the future DR domain (Fig. 16F and supplementary Fig. S1C). In *D. melanogaster*, no similar patterns were found (supplementary Fig. S1A-S1I, and (Yakoby et al., 2008a)).

Figure 16

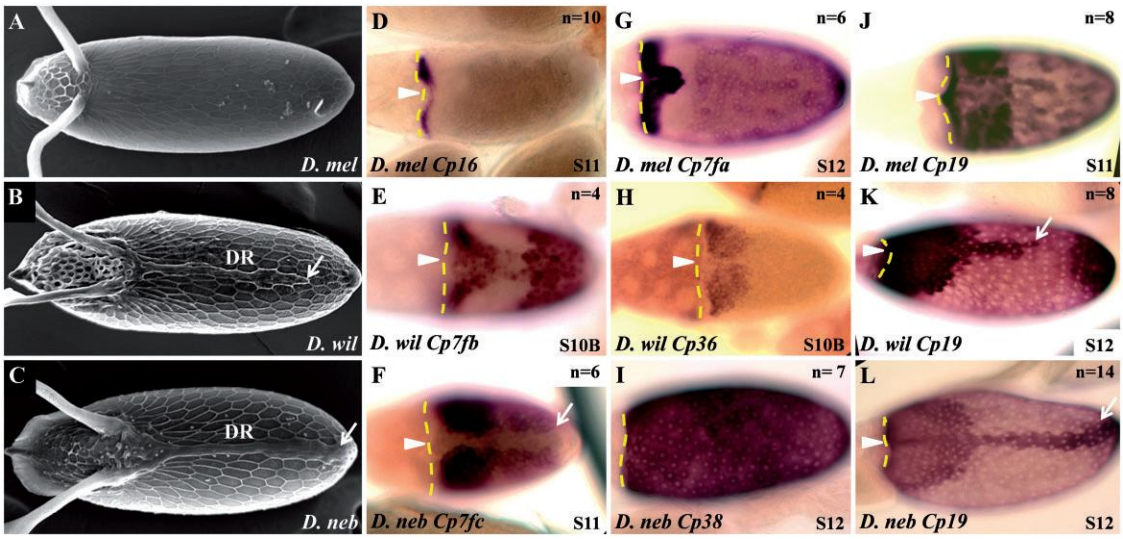

Figure 16: *Drosophila* eggshell morphologies and chorion patterning are diverse. (A–C) Scanning electron images of the wild-type eggshells of *Drosophila melanogaster* (*D. mel*), *D. willistoni* (*D. wil*), and *D. nebulosa* (*D. neb*). The eggshells of *D. wil* and *D. neb* have an additional structure called the DR that begins from the bases of dorsal appendages and extends toward the posterior end along the dorsal-most side of the eggshell (B, C). The DR varies in length between species; the DR of *D. wil* does not reach the posterior end of the eggshell (B, white arrow), while the DR in D. neb reaches the most posterior end of the eggshell (C, white arrow). (D–L) Examples of different patterns of *Cp* genes at different developmental times in the follicle cells of *D. mel*, *D. wil*, and *D. neb*. (F, K, L) Examples of *Cp* gene patterns that reflect DR morphology (white arrow points to the most posterior end of the future DR domain). In all images, broken yellow line denotes anterior region of the follicle cells, white arrowhead denotes dorsal midline, images are dorsal views, and anterior is to the left. The "n" represents the number of similar images to the one that is represented in this figure.

3.2 Transformation of 2D patterning images into digital information

The entire patterning collection includes 108 images (nine *Cp* genes over four developmental stages across three species Fig. S1A-S1I). We were particularly interested in analyzing gene patterning and using gene patterning data to predict which signaling pathways regulate the DR. Previously, a code that is based on six simple shapes of patterning domains that were combinatorially assembled into more complex patterns using Boolean operations, have successfully described the entire 2D image collection of eggshell gene-patterning in *D. melanogaster* (Fig. 8 and (Yakoby et al., 2008a)). This code focuses on the dorsal anterior domain, and thus excludes the posterior domain and the new dorsal ridge domain. Also, this code utilizes a minimal selection of shapes, which are not exclusive. Furthermore, identical patterns can be annotated in various correct ways, which would make computational comparisons between annotations impractical.

To analyze FCs patterning systematically, we used a similar concept, but modified the code to generate exclusive domains that cover the entire follicle cells (Fig. 17Ai and 17Aii). Specifically, in the original code the anterior (A) domain reflects genes that are regulated by BMP signaling, and it spans the cells overlaying the border between the oocyte and the nurse cells (Yakoby et al., 2008a). Here, the A domain is split into the anterior-dorsal (AD) and the anterior-ventral (AV) domains. The midline (M) represents the high levels of EGFR activation and in the original code it includes the AD domain (Yakoby et al., 2008a). Now, the M is separate from the AD. The roof (R) and floor (F) represent two domains that build the top and bottom, respectively, of the future dorsal appendages (Fig. 9 and (Deng and Bownes, 1997; Ruohola-Baker et al., 1993; Ward and

Berg, 2005)). In the original code, the dorsal (D) domain includes AD, M, F, and R. Now, the D domain represents an arch-shaped at the intermediate/low levels of EGFR signaling. The posterior (P) and dorsal ridge (DR) are new shapes that represent the future aeropyle and dorsal ridge domains, respectively. Uniform (U) represents expression throughout the FCs. In addition, we use U as a base to describe the absence of domain expression where patterns are not present. In this way, individual domains can be added on top of, or subtracted from a uniform expression in order to capture domain repression or over-expression.

In the following two examples, we demonstrate the use of the annotation system (Fig. 17B, C, and D). Each pattern is transformed into a binary matrix that scores each domain with 0 or 1 for the absence or presence of expression, respectively. At stage 11, the pattern of *Cp7fc* in *D. willistoni* has a R domain, a U domain that lacks AD, M, F, P, and DR domains (Fig. 17B, B'). At stage 12, *Cp7fc* is expressed in the U domain that lacks the AD and M domains (Fig. 17C, C'). This annotation system enables computational analyses of the entire collection of patterns within and between species. Representing the gene per stage in the rows and the expression domains in the columns, we generated a *Cp* patterning profile for each species (Fig. 17D). Our annotation system captures patterning dynamics in a matrix form, and it generates a spatiotemporal "fingerprint" profile for each species given a set of genes. These matrices can now be analyzed (Niepielko et al., 2014).

Figure 17

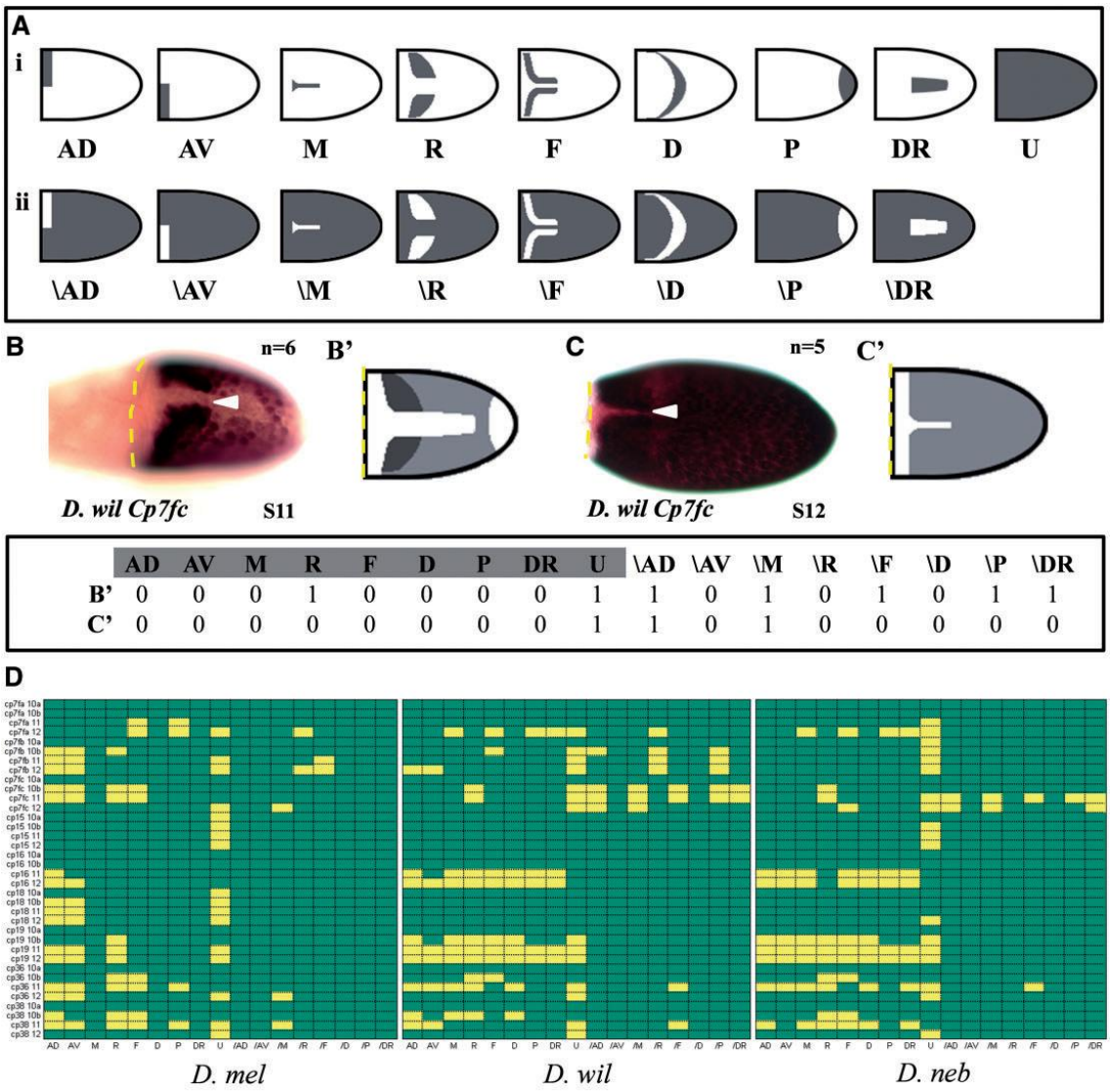

	AD	AV	M	R	F	D	P	DR	U	\AD	\AV	\M	\R	\F	\D	\P	\DR
B'	0	0	0	1	0	0	0	0	1	1	0	1	0	1	0	1	1
C'	0	0	0	0	0	0	0	0	1	1	0	1	0	0	0	0	0

Figure 17: Patterning domains and matrix transformation. (A) Cartoons depicting simple domains observed in follicle cell patterning. (Ai) Domains representing expression. Lateral views: anterior dorsal (AD) and anterior ventral (AV); Dorsal views: midline (M), roof (R), floor (F), dorsal (D), posterior (P), dorsal ridge (DR), and uniform (U). (Aii) Domains representing no expression in a uniform background. (B) transformation of tissue patterning into binary matrices. Each domain in the pattern is given either 1 when present or a 0 for unrepresented. (B, B') The pattern of *Cp7fc* in *D. wil* at S11 is constructed using R, U, \AD, \M, \F, \P, and \DR. (C, C') At S12 *Cp7fc* is characterized as a combination of U, \AD, and \M. (D) Collection of binary matrices for all genes, at all developmental stages, for each species; the rows are the gene/stage, and each column is a specific patterning domain. Arrowhead denotes the dorsal midline and anterior is to the left. Broken yellow line (B, C) denotes the anterior region of the follicle cells.

3.3 The dorsal ridge domain is associated with EGFR signaling regulated domains

Given the range of patterns and diverse use of genes across domains, we next investigated the relationship among expression domains. To determine domain relatedness, we utilized hierarchical clustering of the average expression between the three species (Fig. 18A). We assume that domains that cluster together may be regulated by a similar input. As expected from domains that are regulated by the anteriorly located BMP signaling (Twombly et al., 1996), the AD and AV domains cluster with a bootstrap value of 98% (Fig. 18A).

The P, DR, M, and D domains cluster together with a bootstrap value of 85% (Fig. 18A). This is particularly interesting since the P, M, and D domains are regulated by EGFR signaling (Queenan et al., 1997; Yakoby et al., 2008a), suggesting that the DR domain is regulated in a similar manner. To test the relatedness of DR to EGFR signaling, we looked for a gene that is expressed in M domain; an area with high levels of EGFR activation. Since none of the *Cp* genes is expressed in an M unique pattern in *D. melanogaster* (Fig. 17D), we selected FASIII, a gene that is expressed in the midline of *D. melanogaster* (Shravage et al., 2007; Ward and Berg, 2005) and is a known target of EGFR signaling in the embryo (Dong et al., 1999). In *D. melanogaster*, FASIII is expressed in the AD, M, and F domains (Fig. 18B). In *D. willistoni* and *D. nebulosa*, FASIII is also expressed in the future DR domain (Fig. 18C, D). Interestingly, the patterns of FASIII in the future DR domains reflect the respective length of the dorsal ridge in each species (Fig. 16B, C). In the follicle cells, FASIII was shown to be regulated by BMP signaling (Shravage et al., 2007). Here, activation of EGFR in the posterior domain was sufficient to derive ectopic FASIII expression in this domain (Fig.

18E, E', F, F'). These results support the clustering of the dorsal ridge with other EGFR regulated domain.

Figure 18

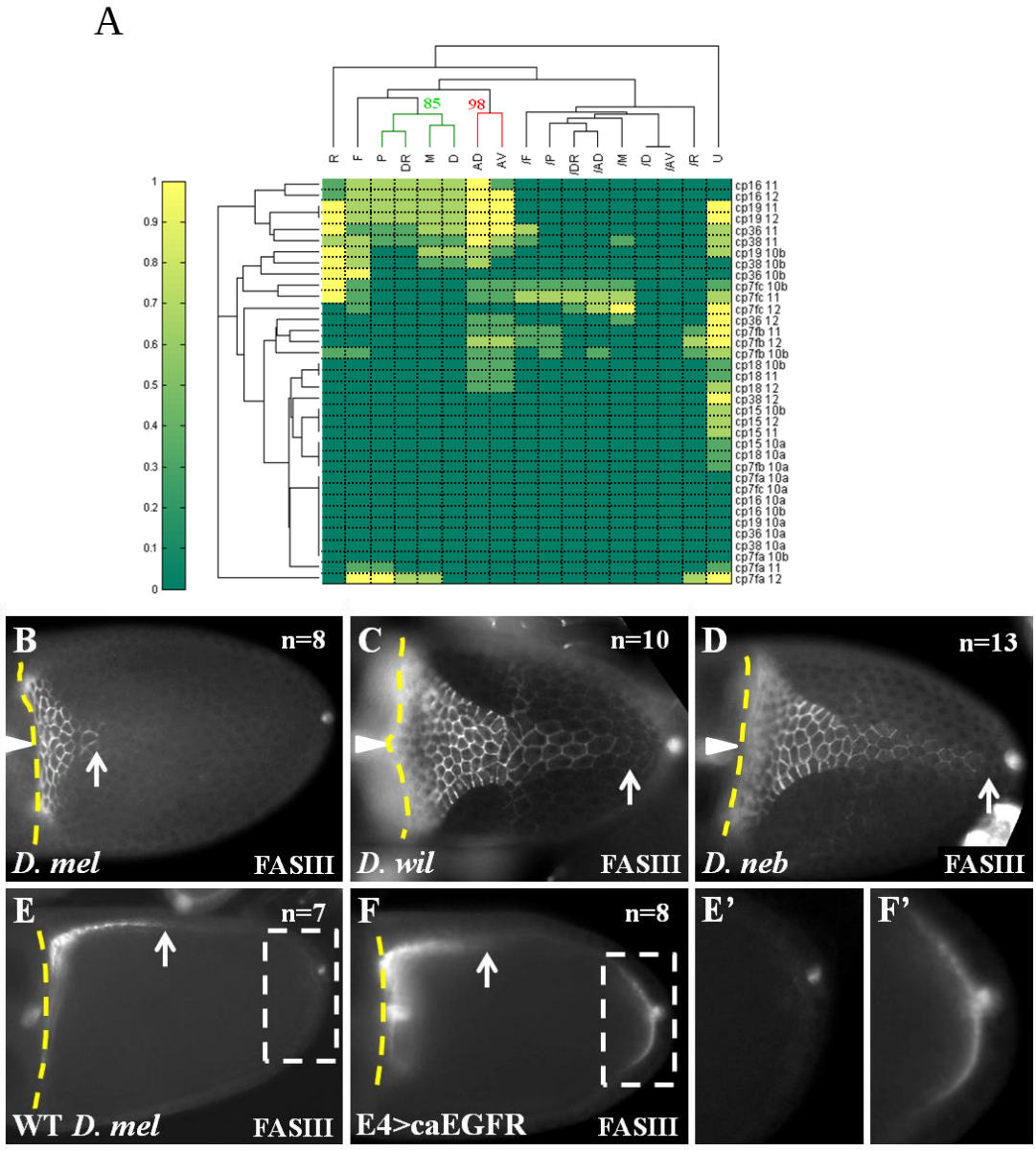

Figure 18: Association of the DR domain with EGFR signaling. (A) Domain relatedness clustergram, values represent bootstrap analysis. Domains are clustered on the top and gene/stage on the left. (B–D) Wild-type expression of FASIII at stage 10B egg chambers in *D. melanogaster* (*D. mel*), *D. willistoni* (*D. wil*), and *D. nebulosa* (*D. neb*). (B) FASIII in *D. mel* is in the dorsal–anterior, midline, and floor domains. (C) In *D. wil*, FASIII is expressed in the dorsal–anterior, midline, floor, and DR domains. (D) In *D. neb*, FASIII is expressed in the dorsal–anterior, midline, floor, and DR domains. (E, E') Sagittal section of FASIII in *D. mel*. (F, F') Posterior activation of EGFR with E4>caEGFR derives ectopic FASIII in the posterior domain. E' and F' are insets that are marked by a white broken line in E and F, respectively. (B–D) Dorsal views. Broken yellow line denotes the most anterior border of the FCs, white arrow points to the most posterior location of FASIII expression, and white arrowhead defines dorsal midline. Of note, posterior polar cells also express FASIII.

3.4 Complex patterns are combinatorially assembled from simple domains

Eggshell patterning is controlled by numerous signaling pathways including EGFR and BMP (Deng and Bownes, 1997; Dobens and Raftery, 1998; Neuman-Silberberg and Schupbach, 1994; Peri and Roth, 2000; Twombly et al., 1996). To determine which domains are controlled by EGFR signaling, using the drug colchicine, we disrupted EGFR signaling by mislocalizing the oocyte nucleus (Peri and Roth, 2000). In *D. melanogaster*, colchicine treatment disrupts dorsal structures including the dorsal appendages and operculum (Fig. 19A). In species with a dorsal ridge, colchicine affected eggshells lack the dorsal ridge and have disrupted dorsal appendages (Fig. 19B, C). Interestingly, in most eggshells of *D. willistoni* and *D. nebulosa*, the dorsal appendages could still be seen, suggesting that the dorsal ridge is more sensitive to changes in the levels of EGFR than the dorsal appendages.

It was previously shown that different domains are regulated by EGFR and BMP pathways independently and cooperatively (Shravage et al., 2007; Yakoby et al., 2008a; Yakoby et al., 2008b). In colchicine treated egg chambers, all patterning domains except for the anterior, uniform, and posterior are disrupted (wild type patterns in Fig. 19D-F compared to colchicine treated flies Fig. 19G-I and Fig. S2A-S2C). This is not surprising since the A and U domains are not regulated by EGFR signaling. The P domain is regulated by EGFR signaling, however, EGFR activation in this domain occurs before nucleus mislocalization. These results are consistent with the patterning changes of these genes when EGFR was activated or repressed uniformly throughout the follicle cells (Fig. S3A-S3C). The anterior domain is regulated by BMP signaling (Twombly et al., 1996; Yakoby et al., 2008a), and thus, we were able to disrupt this domain by overexpressing

the BMP ligand *decapentaplegic* (*dpp*) throughout the follicle cells (Fig. 19J-L and Fig. S3A-S3C). In these cases, the anterior domain expands into a large dorsal dome shaped domain that derives the formation of a large operculum (Twombly et al., 1996; Yakoby et al., 2008a). These results support the idea that complex patterns are combinatorially assembled, and that dorsal ridge patterning is regulated by EGFR activation.

Figure 19

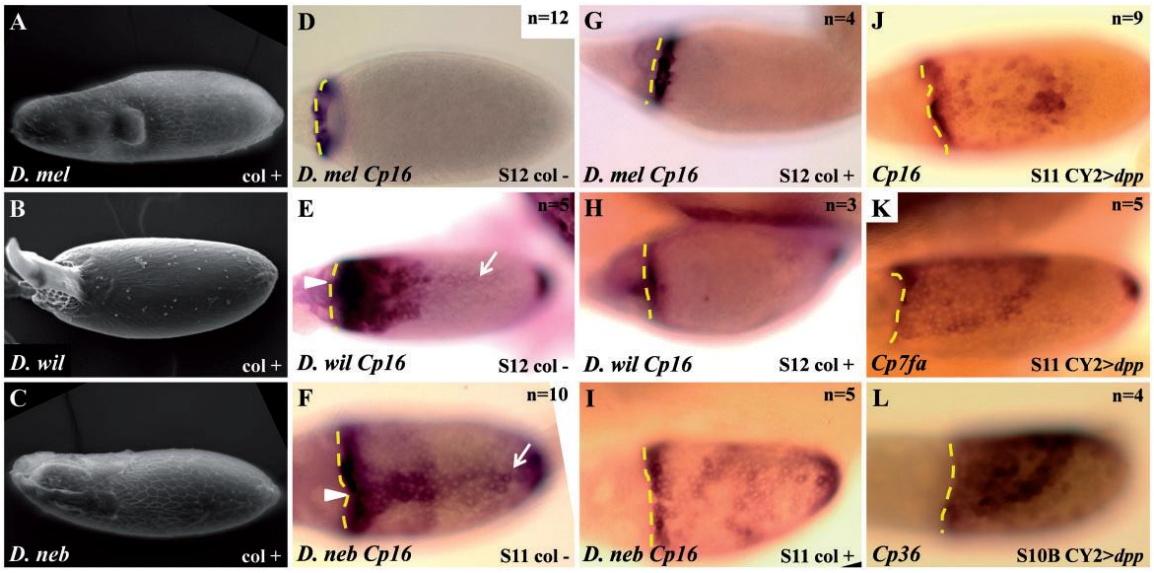

Figure 19: Colchicine disrupts eggshell morphologies and numerous patterning domains. (A–C) Eggs laid by colchicine-treated flies have disrupted eggshell morphologies. (A) The eggshells of *D. melanogaster* lack dorsal appendages. (B) *D. willistoni* eggshells have a fused single dorsal appendage and no DR. (C) *D. nebulosa* eggshells have disrupted dorsal appendages and no DR. (D-F) The wild-type patterns of *Cp16* in *D. melanogaster*, *D. willistoni*, and *D. nebulosa*. (D) *Cp16* is restricted to the anterior domain in *D. melanogaster*. (E) In *D. willistoni*, *Cp16* is patterned in the anterior, midline, roof, floor, dorsal, DR, and posterior domains. (F) Patterning of *Cp16* in *D. nebulosa* includes the anterior, midline, floor, dorsal, DR, and posterior domains. (G–I) *Cp16* patterns in colchicine-treated flies. In all three species, the anterior and posterior patterning domains of *Cp16* are unaffected. In *D. willistoni* and *D. nebulosa*, cochicine treatments affected *Cp16* expression in all other domains including midline, roof, floor, dorsal, and DR (H, I). (J–L) Over expression of *dpp* disrupts *Cp16* (J), *Cp7fa* (K), and *Cp36* (L) dorsal anterior patterns. Broken yellow line denotes the anterior border of the follicle cells, white arrowhead denotes dorsal midline, and white arrow points to most posterior domain of the future DR domain.

Results

Chapter 4: The dorsal ridge: a TGF-alpha-like mediated morphological novelty on the *Drosophila* eggshell

4.1 Dorsal ridge morphologies are consistent with EGFR activation patterns

The DR is a morphologically diverse structure on the eggshells of several *Drosophila* species including Hawaiian *Drosophila* and species within Subgenus *Sophophora* (Margaritis et al., 1983; Niepielko et al., 2014). Absent from *D. melanogaster*, we previously showed that the DR varies in length between *D. willistoni* and *D. nebulosa* (Fig 20A-C and (Niepielko et al., 2014)). Here, we found diversity in the width of the DR. Specifically, *D. cardini*, has a long and narrow DR (Fig. 20D). Similar to the Hawaiian species *D. grimshawi*, *D. cardini* is in subgenus *Drosophilia* (Fig. 20D,E).

Our recent analysis of patterning dynamics and diversities of a family of *Chorion protein* (*Cp*) genes in *D. melanogaster* and two species with a dorsal ridge (*D. willistoni* and *D. nebulosa*), clustered expression patterns spanning the future dorsal ridge domain with expression domains that are regulated by EGFR signaling (Fig. 18) (Niepielko et al., 2014). Together with previous findings that dorsal structures on the eggshell of *D. melanogaster* are regulated by EGFR signaling (Neuman-Silberberg and Schupbach, 1993; Peri and Roth, 2000; Queenan et al., 1997), and that disruption of nuclear localization affects DR formation, we hypothesize that patterns of EGFR activation should be different among species.

Figure 20

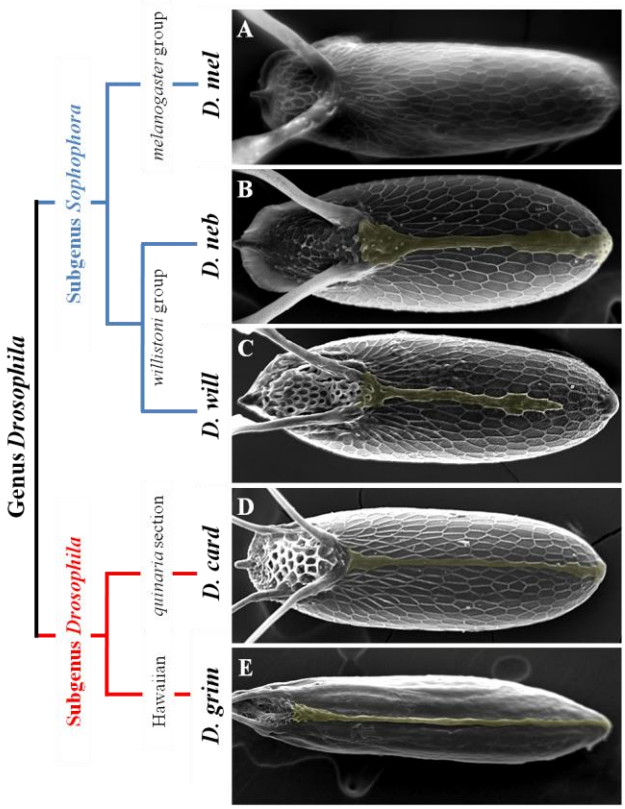

Figure 20: Dorsal ridge morphologies. (A-E) SEM images of eggshells from different *Drosophila* species. The length and width of the dorsal ridge is different among species. (A) *D. melanogaster* (*D.mel*) has no dorsal ridge. (B-E) Eggshells with a dorsal ridge: *D. nebulosa* (*D. neb*), *D. willistoni* (*D. will*), *D. cardini* (*D.card*), and *D. grimshawi* (*D. grim*). The dorsal ridge is artificially colored in yellow for clarity. All eggshells are dorsal views and anterior end is to the left.

To test this hypothesis, we stained egg chambers for dpERK, a downstream target of EGFR activation cascade in wild type flies DR and non-DR flies. The dpERK pattern in *D. melanogaster* is restricted to the dorsal midline (Fig. 21A). As predicted, in dorsal ridge species, dpERK extends from the most dorsal anterior domain of follicle cells overlying the oocyte towards the posterior end (Fig. 21B-D). Interestingly, the patterns of dpERK in species with a dorsal ridge reflect the final shape and size of the dorsal ridge morphologies. Specifically, the pattern of dpERK in the future dorsal ridge domain is wider in *D. nebulosa* and *D. willistoni* than *D. cardini* (Fig. 21B-D). In addition, we note that dpERK patterning extends to the most posterior FCs in *D. nebulosa* and *D. cardini*, but not in *D. willistoni* (Fig. 21B-D). These findings are consistent with the expression patterns of *Cp* genes in the future dorsal ridge domain, which reflect the final shape and

size of the dorsal ridge (Fig. 16K, L)(Niepielko et al., 2014). We conclude that the activation pattern of EGFR in the future dorsal ridge domain is consistent with the final dorsal ridge morphology.

Figure 21

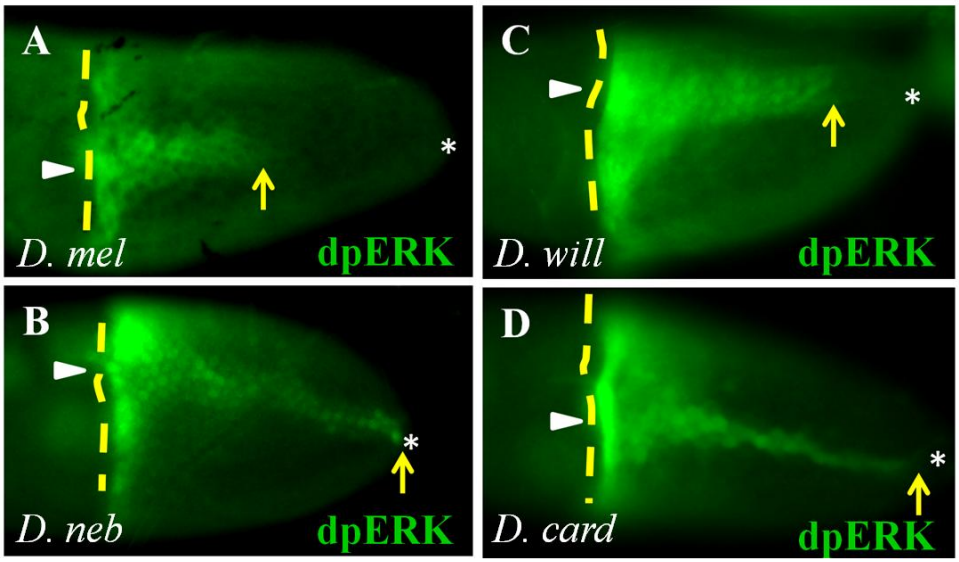

Figure 21: Dorsal ridge morphologies are consistent with the patterns of EGFR activation. (A-D) Dorsal views of EGFR activation in *D. mel*, *D. neb*, *D. will*, and *D. card*, detected by dpERK (green). Patterns of dpERK are consistent with dorsal ridge morphology (Fig. 20). White arrowhead denotes the dorsal midline. Broken yellow line represents the anterior follicle cells overlaying the oocyte. Yellow arrow denotes the most posterior region of dpERK pattern, and the asterisk represents the most posterior region of the oocyte. In all images, anterior is to the left.

4.2 Gurken distribution is consistent with EGFR activation patterns

The pattern of dpERK in the dorsal ridge domain is an indication that a localized ligand activates EGFR in a restricted manner. During *D. melanogaster* oogenesis, the *grk* mRNA is produced in the germline and localizes near the oocyte nucleus. The localized *grk* serves as a source of GRK proteins that is translated and secreted to the perivitelline space, where it generates an activation gradient of EGFR in the overlaying follicle cells (Neuman-Silberberg and Schupbach, 1993; Thio et al., 2000). The mRNA of oocyte secreted TGF-α like ligands in other animals, including *Tribolium* (beetle) and *Gryllus* (cricket), are not strictly localized near the oocyte nucleus (Lynch et al., 2010). Given

the unique patterns of EGFR activation, we hypothesized that *grk* mRNA is differently distributed in species with a dorsal ridge. To test this hypothesis, we analyzed the pattern of *grk* in the four species. Like *D. melanogaster*, *grk* is localized near the oocyte nucleus in all tested species (Fig. 22 and Fig. 23A-C). These results are consistent with the conserved localization of *grk* in *D. virilis*, a species that is 45 million years apart from *D. melanogaster* (Peri et al., 1999). Thus, the localization of *grk* is conserved across all tested species, demonstrating that the differences in EGFR activation are not due to changes in *grk* RNA localization.

Figure 22

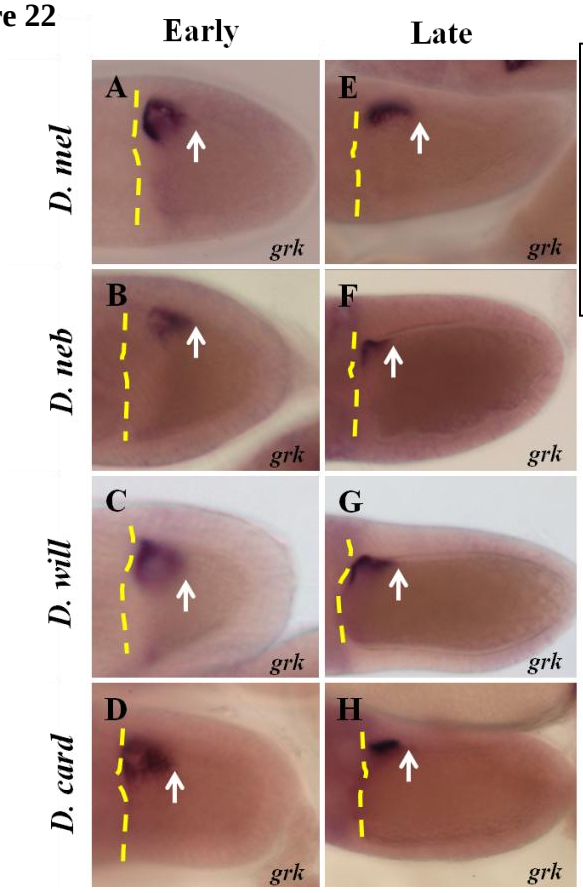

Figure 22: Expression pattern of *grk* across *Drosophila* species. Expression pattern of *grk* in *D. melanogaster* (*D. mel*), *D. nebulosa* (*D. neb*), *D. willistoni* (*D. will*), and *D. cardini* (*D. card*) at stage 9 (Early, A-D) and 10A (Late, E-H) of oogenesis. All images are sagittal sections and anterior is to the left.

Next, we aimed to determine whether the localization of GRK protein can account for the patterns of dpERK in species with and without a dorsal ridge. The pattern of GRK in *D. melanogaster* is well characterized (Neuman-Silberberg and Schupbach, 1994; Van

Buskirk and Schupbach, 1999). At stage 9, the GRK protein is localized near the nucleus of the oocyte and extends towards the posterior (Fig. 23D, D', E). Since the available anti GRK antibody is specific to *D. melanogaster*, we produced *D. willistoni* and *D. cardini* anti GRK antibodies. Using these antibodies, we found a clear difference in the distributions of GRK among species. Specifically, in *D. willistoni* and *D. cardini*, in addition to being localized near the oocyte nucleus, GRK extends to the posterior in the perivitelline space (Fig. 23F-I). Furthermore, the pattern of GRK stops short near the posterior end of *D. willistoni* (Fig. 23F, F', and G). These patterns reflect the shapes and lengths of dpERK and the final dorsal ridge structures in the corresponding species (Fig. 20 and Fig. 21). Of note, the new antibodies recognize GRK only in the corresponding species

Figure 23

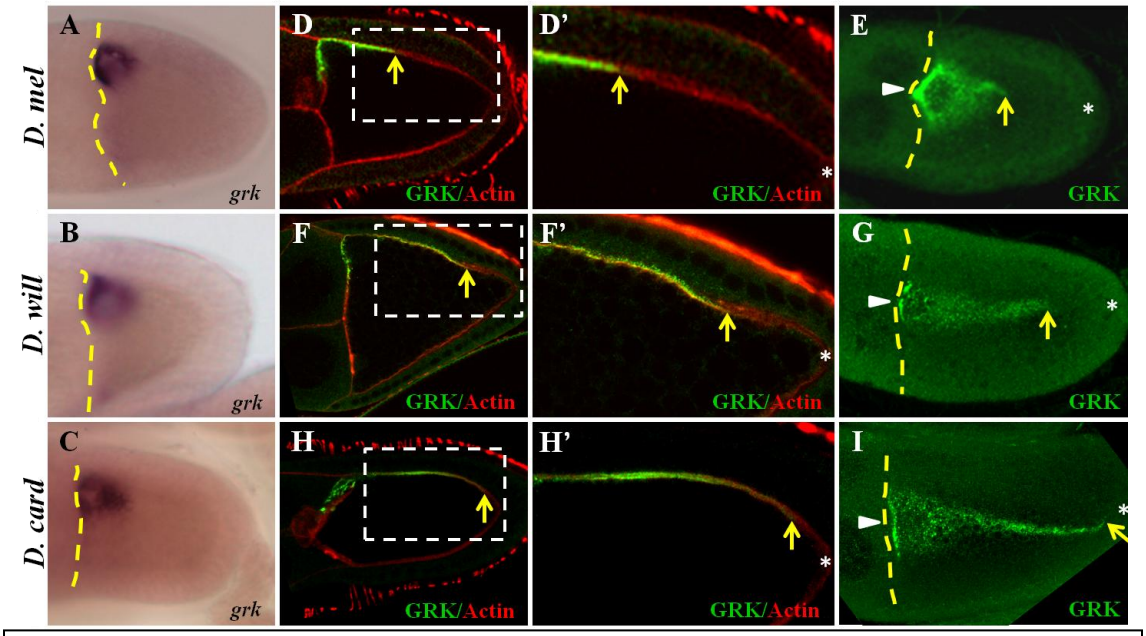

Figure 23: Localization of Gurken protein is different among species. (A-C) Sagittal view of *gurken* mRNA (*grk*) shows that it localizes near the oocyte nucleus of all tested species. Sagittal (D,F, H) and dorsal views (E, G, I) of stage 9 egg chambers stained for Gurken protein (GRK) (green) and Actin (phalloidin – red). (D, D') In *D. melanogaster* (*D. mel*), GRK is localized near the nucleus with a short elongation towards the posterior. (F, F', H, H') In species with a dorsal ridge, in addition to being localized near the nucleus, GRK is also extending towards the posterior end of the FCs along the dorsal most side of the oocyte. D', F', and H' are the insets marked by white dotted box in D, F, and H, respectively. Broken yellow line denotes the anterior FCs overlaying the oocyte. Yellow arrow denotes the most posterior region of GRK pattern. In all images, anterior is to the left. Arrowhead denotes the dorsal midline.

4.3 GRK is necessary for dorsal ridge formation

To associate GRK directly with dorsal ridge formation, we knocked down *grk* in *D. willistoni* and *D. melanogaster* using species-specific RNAi constructs (Fig. 24A). This method was used successfully to disrupt the TGF-α like ligand in the oocyte of the beetle, wasp, and cricket (Lynch et al., 2010). Due to the low efficiency of germline GAL-4 drivers, we took advantage of the minimal heat shock promoter to drive the expression the *grk* RNAi constructs (see M&M for details). In *D. melanogaster*, we observed three types of dorsal appendage phenotypes; severe (5%), fused (68%), and wild type (27%) (Fig. 24B-D). Over 70% of the heat shock treated eggshells had some levels of disrupted dorsal appendages. The controls, heat shocked wild type flies and *grk* RNAi flies kept at 18C, were mostly wild type eggshells (Fig. 24*i*). These results are consistent with eggshell phenotypes of disrupted EGFR activation (Neuman-Silberberg and Schupbach, 1993).

In heat shock treated *D. willistoni,* we observed three types of eggshell morphologies. As expected, the dorsal ridge was disrupted in 85% of the eggshells (Fig. 24E-G). In 51% of the eggshells, the dorsal ridge is absent (Fig. 24E). In 34% of the eggshells, a few constricted cells near the base of the dorsal appendages can be seen with reduced secretion of chorion material (Fig. 24F). Wild type appearance was observed in only 15% of the eggshells (Fig. 24G). Of note, eggshells from heat shocked treated *D. willistoni* wild type flies were also affected, however, the moderate and wild type phenotypes were the majority (81%) (Fig. 24*ii*). When *grk* RNAi flies were kept at 18C, 98% of the eggshells were wild type. The RNAi treatment successfully reduced the levels of GRK and dpERK (Fig. 25B, D), further supporting that GRK is necessary for dorsal

ridge formation, which is in agreement with the obtained phenotypes of colchicine treated flies (Niepielko et al., 2014).

Figure 24

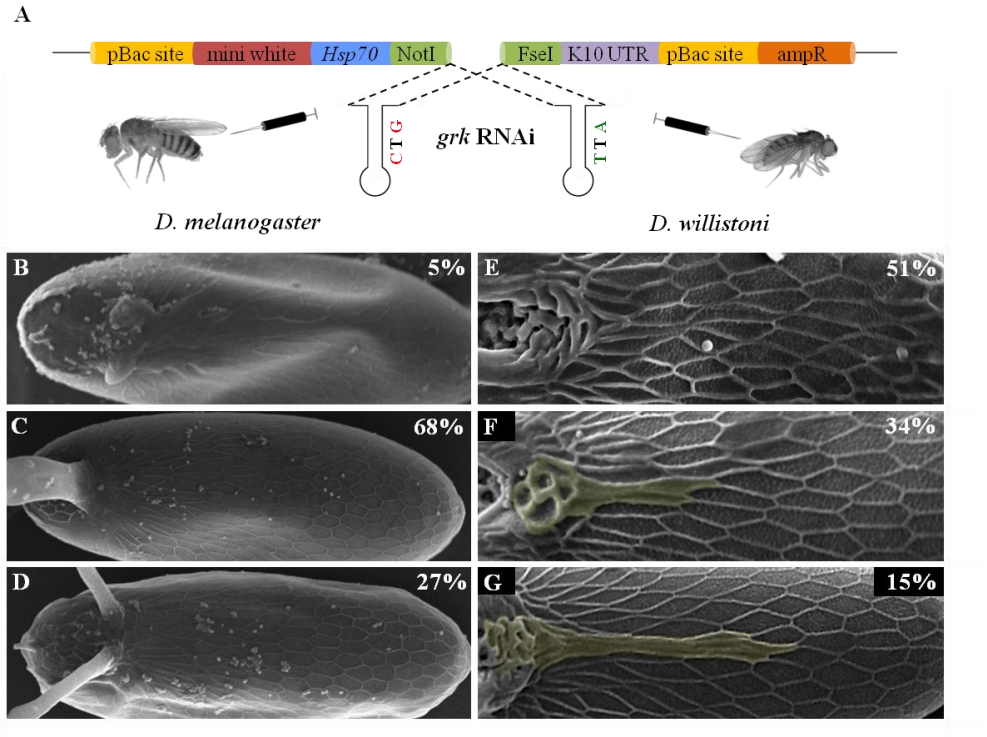

gurken RNAi Phenotypes

i

	D. mel grk RNAi	D. mel control	RNAi 18C
Extreme	5%	2%	17%
Moderate	68%	20%	12%
Wild Type	27%	78%	71%
Counts	n=194	n=113	n=122

ii

	D. will grk RNAi	D. will control	RNAi 18C
No DR	51%	19%	2%
Moderate	34%	38%	0%
Wild Type	15%	43%	98%
Counts	n= 134	n= 164	n= 117

Figure 24: Gurken RNAi disrupts eggshell morphologies. (A) A schematic representation of the UASpBacNPF injection vector (Holtzman et al., 2010) used to carry the *grk* RNAi constructs for *D. melanogaster* (left) and *D. willistoni* (right). The two nucleotide differences between the two *grk* RNAi constructs are denoted in red and green. Eggshell phenotypes of transgenic knockdown of *grk* in *D. melanogaster* (B-D) and *D. willistoni* (E-G). The knockdown of GRK in *D. melanogaster* produced three types of eggshells: (B) Extreme, no dorsal appendages. (C) Moderate, fused appendages, and (D) Wild type looking. The knockdown of GRK in *D. willistoni* produced three types of eggshells: (E) Extreme, no dorsal ridge. (F) Moderate, incomplete dorsal ridge. (G) Wild type looking dorsal ridge. All eggshells are dorsal views with anterior to the left. Dorsal ridge is artificially yellow colored for clarity. The percents are calculated out of total counts of 194 and 134 eggshells of *D. melanogaster* and *D. willistoni*, respectively.

Figure 25

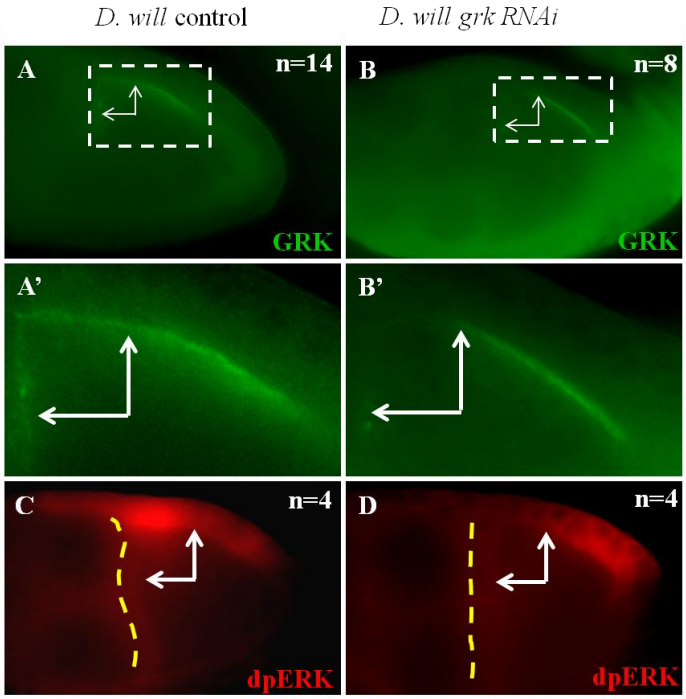

Figure 25: *D. willistoni* flies affected by *grk* RNAi have disrupted GRK and dpERK patterns. (A) The wild type pattern contains GRK protein directly near the nucleus (white arrows in A and A'). A' is an inset denoted by a broken white line box in A. (B) The pattern of GRK in *grk*RNAi affected egg chambers is reduced in the area around the nucleus (white arrows in B and B'). B' is an inset denoted by a broken white line box in B. A and B are sagittal views of stage 8 egg chambers with the anterior to the left. (C) Sagittal view of dpERK staining in wild type *D. willistoni* (white arrows in C). (D) Sagittal view of dpERK staining in *D. willistoni* in *grk*RNAi affected egg chambers. dpERK is reduced in the area around the nucleus (white arrows in D). All images anterior is to the left. Yellow broken line denotes the anterior border of the oocyte associated follicle cells.

4.4 *D. willistoni grk* rescues *D. melanogaster grk* null and is sufficient to form a dorsal ridge-like structure

The *grk* gene is rapidly evolving among *Drosophila* species and outside of Diptera (Lynch et al., 2010), thus it is not surprising that anti GRK antibodies (available for *D. melanogaster* and two additional in this project) are species-specific. Homology among *grk* genes is restricted to a few domains, including the signal peptide and EGF binding domain (Peri et al., 1999), thus it is uncertain whether *grk* from one species can be processed correctly and rescue another. Previously, germline cells were exchanged between *D. virilis* and *D. melanogaster*, however, the progeny contained *grk* from both

species (Nakamura et al., 2007). As a first step, we wanted to determine whether *grk* from *D. willistoni* (*w*GRK) localizes correctly in *D. melanogaster* oocyte. For that, we injected the entire *grk* locus from *D. willistoni* into *D. melanogaster* (Fig. 26A). We found that *w*GRK RNA and protein are correctly localized to a dorsal anterior in the transgenic *D. melanogaster* fly (Fig. 27). Thus, the localization, intracellular processing, and secretion of *w*GRK are properly working in *D. melanogaster*.

Next, we aimed to determine the function of the transgenic *w*GRK in *D. melanogaster* eggshell morphology. For that, we crossed the transgenic *w*GRK fly into a *grk* null fly, obtaining progeny with one or two copies of *w*GRK in a *grk* null background. Four distinct eggshell phenotypes were obtained, and the distribution of these phenotypes differed between one and two copies of *w*GRK (Fig. 26B). Most eggshells, 69% and 78% from one and two copies of *w*GRK, respectively, were Class I (wild type) and Class II (wild type with enlarged area between the two dorsal appendages). As far as we know, this is the first time it has been demonstrated that *grk* from a different species can rescue a *grk* null of *D. melanogaster*. Remarkably, in 10% and 1% of the eggshells from one and two copies of *w*GRK, respectively, a dorsal ridge-like morphology was found (Fig. 26B, III). The cross section of the dorsal ridge-like structure was compared to the WT dorsal ridge cross sections of *D. nebulosa* and *D. willistoni* and was found to be structural similar (Fig. 28).

In 13% and 18% of the eggshells from one and two copies of *w*GRK, respectively, we noticed a single/fused dorsal appendage (Fig. 26B, Class IV). Of note, in 8% and 3% of the one and two copies, respectively, the eggshells were completely disrupted and could not be mounted (sever phenotype – not shown). The low penetrance

of eggshells with a dorsal ridge is consistent with the few egg chambers found to have elongated distribution of *w*GRK along the future dorsal ridge domain (Fig. 27E, E').

Figure 26

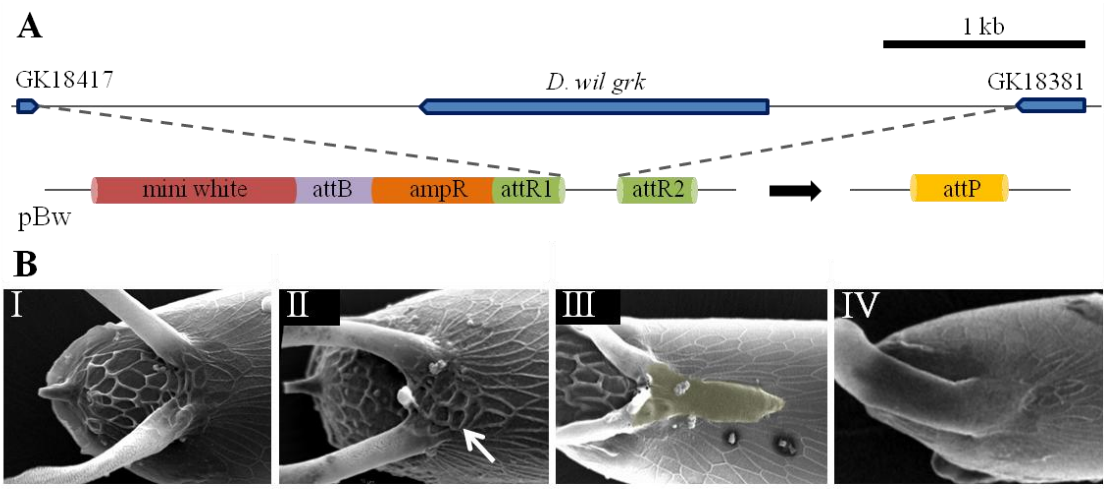

	Class I	Class II	Class III	Class IV	Severe
1x *wgrk* rescue n = 337	69%	0%	10%	13%	8%
2x *wgrk* rescue n = 491	47%	31%	1%	18%	3%

Figure 26: *D. willistoni grk* (*w*GRK) rescues a *grk* null fly of *D. melanogaster*. (A) The entire *grk* locus of *D. willistoni* (*wGRK*) was inserted into a modified pBPGUw (pBw), and injected into *D. melanogaster* at position 68A4 of the attP2 fly (Genetic Services, MA). Transgenic flies were crossed to a *grk* null background. (B) Eggshells of transgenic flies showed four phenotypic classes. I – Wild type, II – Enlarged area between the dorsal appendages, denoted by a white arrow. III – Dorsal ridge-like structure (artificially yellow colored for clarity). IV – A single dorsal appendage. The table on the bottom summarizes the phenotypic distributions of eggshells to the four classes in flies with one additional copy of *w*GRK (1x *wgrk* rescue) and two copies (2 x *wgrk* rescue). Both one and two copies of *w*GRK are in a *grk* null background. Images are dorsal views and anterior is to the left.

Figure 27

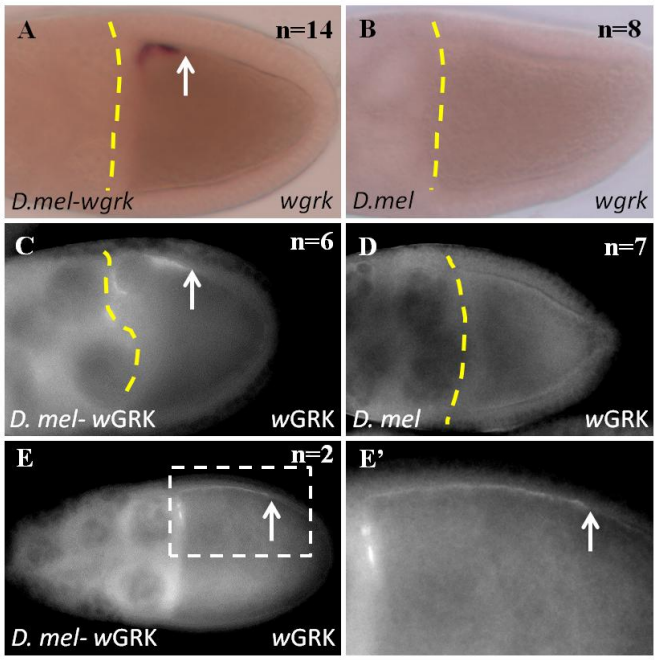

Figure 27: *w*GRK localizes correctly in *D. melanogaster*. (A) Probe against *wgrk* detects correct RNA localization near the oocyte nucleus of transgenic *D. melanogaster*. (B) The same probe fails to detect the *grk* RNA in wild type *D. melanogaster*. (C) An antibody against *w*GRK detects the correct localization of *w*GRK in a *w*GRK transgenic *D. melanogaster*. (D) The same antibody fails to detect GRK in *D. melanogaster*. (E, E') In a few cases, we noticed a dorsal elongated pattern of the *w*GRK protein, similar to its distribution in *D. willistoni*. Yellow broken like denotes the anterior border of the oocyte associated FCs, white arrow points to the most posterior region of *grk* and GRK. All images are sagittal views and anterior is to the left.

Figure 28

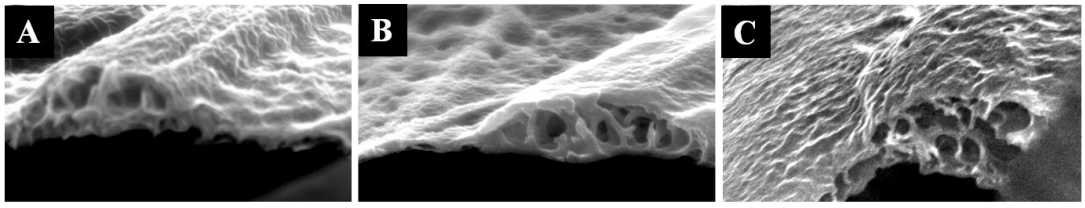

Figure 28: Cross sections of the DR in *D. neb, D. will,* and the wGRK rescue fly. The dorsal ridge is structurally similar in *D. neb, D. will,* and the wGRK rescue fly.

Chapter 5: Discussion and Future Directions

We address fundamental questions surrounding the underlying mechanisms guiding the evolution of morphology using the morphological diversity displayed by the eggshells of *Drosophila* species (Hinton, 1981; Kagesawa et al., 2008; Nakamura and Matsuno, 2003; Niepielko et al., 2011). With respect to DA structures, we found patterning changes to the BMP type-1 receptor, *tkv*, are sufficient to produce the diverse BMP signaling patterns found in nature. Furthermore, we found that the TGF-α-like ligand, GRK, mediates dorsal ridge formation through EGFR signaling. While the molecular mechanisms controlling morphological diversity are mostly unknown (Carroll, 2005, 2008), our results support the idea that changes in major signaling pathway components, including receptors and ligands, underlie the evolution of morphologies.

5.1 Shaping the BMP signaling gradient with TKV expression levels

The regulation of BMP signaling dynamics by TKV was studied in the FCs of *D. melanogaster* (Lembong et al., 2009; Yakoby et al., 2008b). In a follow up study, a comprehensive analysis of BMP signaling activation was carried out in the FCs of multiple *Drosophila* species (Niepielko et al., 2011). The latter aimed to explore whether the mechanism controlling signaling dynamics in *D. melanogaster* is conserved across species. The idea that changes in a single component can vary the pattern of signaling was particularly intriguing since the BMP pathway is comprised of multiple components. Indeed, modifications in some of these components led to changes in the pattern of signaling in other experimental systems (Abzhanov et al., 2004; Fuentealba et al., 2007; Goltsev et al., 2007; O'Connor et al., 2006). In addition, these *Drosophila* species represent major clades in the genus *Drosophila* and span ~35 million years of speciation.

Here, we explored the functions of TKV in shaping the gradient of BMP signaling and its sufficiency to diversify the patterns of signaling activation across species.

The proposal that levels of TKV control gradients of BMP signaling was studied computationally and tested experimentally. The mathematical model predicts that an increase in φ value, which depends on the levels of the receptor (R), will sharpen the gradient of signaling activation closer to the ligand source. This model is supported by the gradual increase in the levels of TKV that was adequate to progressively restrict BMP signaling to the anterior domain (Fig.13). Further support for this model was obtained by the analysis of loss of function (LOF) clones of *tkv* in FCs. These clones generate mosaic tissue comprised of groups of cells that are null (zero copies), heterozygous (a single copy), and homozygous (two copies) for *tkv*. Interestingly, groups of cells with two copies of *tkv* had higher signaling levels than neighboring cells with a single copy (Yakoby et al., 2008b); possibly due to higher levels of TKV available to sequester DPP (Schwank et al., 2011). We conclude that levels of TKV control the activation gradient of BMP signaling.

The role of TKV in shaping the gradient of BMP signaling activation has been studied thoroughly in imaginal discs during larvae development (Affolter and Basler, 2007; Schwank et al., 2011). In the haltere, DPP signals near the A/P boundary, at the source of DPP secretion (Crickmore and Mann, 2006). The short range activation of BMP signaling is attributed to the uniform expression of TKV throughout the haltere. Likewise, the early pattern of *tkv* expression is uniform throughout the FCs (Mantrova et al., 1999). This pattern can account for the restricted pattern of early BMP signaling near the anterior source of DPP (Dequier et al., 2001; Peri and Roth, 2000; Shravage et al.,

2007; Twombly et al., 1996). In contrast, in wing imaginal discs, DPP signals in cells that are away from the source of DPP (Lecuit et al., 1996). In this case, the repression of TKV in the A/P boundary allows DPP to signal in more distant cells (Lecuit and Cohen, 1998). Similarly, in stage 10B egg chambers, the width of BMP signaling activation is ~5 cells in the dorsal midline domain and ~2 cells in lateral and ventral domains (Niepielko et al., 2011; Yakoby et al., 2008b). The broader midline signaling reflects the repression of *tkv* in this domain (Mantrova et al., 1999; Yakoby et al., 2008b) which, we propose, reduces the levels of the TKV receptor and allows DPP to diffuse and signal more posteriorly (Fig. 13).

Support for this model was obtained by over-expressing *tkv* throughout the FCs that prevented signaling from acquiring DV polarity at later stages of egg development (Niepielko et al., 2011). In addition, in FCs with large *tkv* LOF clones, P-MAD was found in posterior cells that do not signal in the wild type (Yakoby et al., 2008b). We suggest that removal of *tkv* from the dorsal midline domain enables DPP to travel more posteriorly. A similar mechanism was found in wing imaginal discs, where DPP can travel through a field of cells null for *tkv* and signal in more distant domains (Schwank et al., 2011). Interestingly, the transition of BMP signaling from being restricted to the anterior domain to a pattern with D/V polarity is conserved in the FCs of multiple species (Niepielko et al., 2011). Through evolution, many *Drosophila* species maintained the ability to temporally regulate the range of DPP diffusion in the follicular epithelium by regulating the pattern of *tkv* (Niepielko et al., 2011). We propose that this mechanism is conserved through *Drosophila* speciation, and it depends on the repression of *tkv* in the dorsal midline.

The mechanisms by which different spatial patterns of *tkv* are regulated across species are still unknown; however, we propose that changes in *cis*-regulatory modules, which govern the spatial expression of *tkv*, as a potential mechanism (Gordon and Ruvinsky, 2012). In the FCs of *D. melanogaster*, ectopic expression of *tkv* in distinct domains is sufficient to recapitulate the different patterns of BMP signaling found in the FCs of other species (Niepielko et al., 2011).

5.2 Future work involving *tkv*

Beyond the evolutionary mechanisms underlying signaling diversification, we would like to understand the phenotypic consequences of qualitative and quantitative changes in BMP signaling. Previously, we found that repression of the anterior domain of BMP signaling led to reduction in operculum size and deformed the DAs' morphologies (Yakoby et al., 2008b). We also found that the depletion of TKV from the future roof domains deforms DAs formation by affecting their morphogenetic process (Niepielko et al., 2011). At the same time, we could not detect obvious morphological changes after expressing *tkv* in the floor domain. In the future, it will be desirable to perturb *tkv* in multiple species to fully understand its evolutionary role in modulating signaling domains and levels of signaling within these domains. Special attention for the role of TKV in eggshell morphogenesis is required in species with different eggshells. Specifically, late BMP activation is observed in the floor domain in species such as *D. willistoni* and in the anterior domain in species such as *D. virilis.* Since the late Phase of BMP signaling on the roof domain has been associated with DA morphogenesis in *D. melanogaster* (Niepielko et al., 2011), it will be interesting to investigate the removal of *tkv* in the floor

and anterior domains in other species to determine the functional role of BMP signaling in these specific regions.

5.3 New approach to analyzing dynamics and diversities of tissue patterning

Two main signaling pathways pattern the *Drosophila* eggshell, the EGFR and BMP (Berg, 2005). These pathways act independently and cooperatively to pattern different domains of the eggshell (Yakoby et al., 2008b). The early activation pattern of both pathways is highly conserved across multiple species (Kagesawa et al., 2008; Niepielko et al., 2011; Niepielko et al., 2012). In contrast, the late activation patterns are different. In particular, the late pattern of EGFR activation reflects the number of dorsal appendages (Kagesawa et al., 2008), whereas the late pattern of BMP signaling is highly associated with the species' phylogeny (Niepielko et al., 2012).

Here, we introduced a new approach to analyze the dynamics and diversities of genes that pattern the follicular epithelium by converting 2D images into digital format (Niepielko et al., 2014). We focused on the family of *Cp* genes that have a highly conserved protein sequences and structures across fly species (Waring, 2000). Analyzing *Cp* genes' patterning across fly species with different eggshell morphologies allowed us to address fundamental questions regarding the relationship among patterning, gene regulation, and cell signaling.

5.4 Patterning domains are linked to the signaling inputs

To determine how expression domains associate in different species and to give insight into the underlying signals, we altered a previously developed code to annotate gene-patterning of *D. melanogaster* eggshell (Yakoby et al., 2008a). The new code has exclusive domains, which allows for the generation of binary matrices that can be

analyzed for patterning differences among species in an unbiased manner and includes the posterior and new dorsal ridge domain. The patterns of *Cp* genes are dynamic and diverse amongst species and using the idea that domains expressed at the same time may be regulated by similar inputs, we clustered expression domains and determine that EGFR regulated domains are co-expressed with the dorsal ridge (Niepielko et al., 2014).

5.5 Patterns are combinatorially assembled and reflect species relatedness

Gene patterning reflects different inputs that converge on the regulatory region of genes. Our genetic and chemical perturbations could differentially disrupt patterning domains. For example, perturbations in EGFR signaling disrupted most domains except for the anterior domain, which was disrupted by perturbations in BMP signaling (Fig. 19 J, K, L, S3A-C). Interestingly, a short fragment of regulatory DNA (84 bp) from the *Cp36* gene was able to recapitulate the full pattern of the gene (Tolias et al., 1993). By examining the two halves of this fragment, they successfully separated the anterior and posterior expression domains of the gene. These results further support our previous analysis of multiple gene patterns in *D. melanogaster*, which suggested that gene patterns are assembled combinatorially by inputs from different pathways (Yakoby et al., 2008a).

5.6 Regulation of eggshell structures by different levels of EGFR signaling

The extension of the operculum beyond the base of the dorsal appendages with two copies of *w*GRK (Fig. 26B, Class II) and the formation of a dorsal ridge in the same domain in flies with one copy of *w*GRK (Fig. 26B, Class III) suggest that dorsal ridge and operculum formation are regulated by different levels of EGFR signaling. In this case, we speculate that the operculum domain is affected by high levels of EGFR signaling mediated by the nucleus emanating GRK, whereas, dorsal ridge is regulated by

lower levels of signaling mediated by the source of GRK from the future dorsal ridge domain.

5.7 Evolutionary changes to GRK sequences and trans acting elements may play important roles in GRK patterning

Sequence comparison between *D. melanogaster* and *D. willistoni* GRK proteins reveals that the main functional domains, including the signal sequence and EGF binding domain are highly conserved (not shown). While *w*GRK is sufficient to induce dorsal ridge formation in *D. melanogaster*, we could not find a protein domain that may explain the difference between *m*GRK and *w*GRK. Since *m*GRK cannot induce dorsal ridge in *D. melanogaster*, a detailed analysis of the two proteins is needed to determine which domain in *w*GRK mediates the distributions of GRK along the future dorsal ridge domain.

Another consideration is the presence of trans acting elements affecting GRK distribution. Specifically, several mechanisms were shown to regulate EGFR signaling, including negative regulators, extracellular matrix proteins, and co-receptors (Boisclair Lachance et al., 2009; Mao and Freeman, 2009; Wang et al., 2008; Zartman et al., 2009). It was shown that Fasciclin 2 (FAS2) is a negative regulator of EGFR signaling (Mao and Freeman, 2009). Notably, the extracellular matrix protein FAS3 is expressed along the dorsal ridge domain (Niepielko et al., 2014).

5.8 Future directions for EGFR signaling

Evidence suggest that there is regulation of eggshell structures by different levels of EGFR signaling. In the future, it will be important to determine what levels of EGFR activation are needed to specify different eggshell structures. Adding additional copies of

*w*GRK to *D. willistoni* may provide information about how higher levels of EGFR signaling may affect dorsal ridge and operculum morphologies.

Since *w*GRK was able to produce a dorsal ridge-like structure in 10% of the rescue eggshells, it will be interesting to investigate trans-acting elements that may provide local regulation of GRK distribution or EGFR signaling. Such candidates include Fasciclin, Dally-like, Dally, and EGFR inhibitors.

Chapter 6: MATERIALS AND METHODS

6.1 Flies, genetic and chemical manipulations:

The following *Drosophila* species were used: *D. erecta, D. tropicalis, D. quinaria, D. cardini, D. willistoni, D. willistoni* pBac-Blue eye (Holtzman et al., 2010) (UC San Diego *Drosophila* Stock Center), *nebulosa* (a gift from D. Stern) and *D. melanogaster* (wild-type OreR*), w*$^{-}$ *D. melanogaster* grk null [2b]*b, grk* null [2E12]*b* (gifts from Trudi Schüpbach), *w*$^{-}$ *D. melanogaster* and 68A4 of the attP2 fly (Genetic Services, MA). Additional fly stocks included *rho*-GAL4 and *rho*-LacZ (a gift from F. Hassinger and C. Berg), CY2-GAL4 and 55B-GAL4 (Queenan et al., 1997), *br*-GAL4 (a gift from H. Cui and L. Riddiford), UAS-*tkv*RNAi (VDRC), and UAS-*tkv*1-3B3 (a gift from M. O'Connor), E4-Gal4, and UAS-caEGFR (Queenan et al., 1997), USA-*dpp* and UAS-dnEGFR (Peri and Roth, 2000). All flies were maintained on standard cornmeal food. Scaffolding was used for maintaining non *D. melanogaster* species. Baker's yeast was added to the food 24 hours prior to ovary collection. Over activation of EGFR signaling in the posterior FCs was achieved by driving UAS-caEGFR with E4-Gal4. Ectopic expression of *tkv* in cells adjacent to Broad (BR) cells was achieved by driving UAS-*tkv*1-3B3 with *rho*-GAL4. Weak and strong overexpressions of *tkv* in the FCs were carried out by driving UAS-*tkv*1-3B3 with 55B-GAL4 and CY2-GAL4, respectively. Depletion of *tkv* from the BR cells was carried out by driving a UAS-*tkv*RNAi with *br*-GAL4. Uniform over-expression of BMP and EGFR signaling was completed using CY2-Gal4 to drive USA-*dpp* and UAS-caEGFR respectively. Uniform reduction in EGFR signaling by using CY2-Gal4 to drive UAS-dnEGFR. *D. melanogaster, D. cardini,* and *D. willistoni* flies were fed colchicine mixed with a yeast paste (25ug/ml) for

24 hours prior to dissection and eggs collection as previously described (Peri and Roth, 2000). Colchicine treatment for *D. nebulosa* was carried out for 48 hours at the same concentration. Colchicine treatment indirectly mislocalizes EGFR signaling by destabilizing microtubules involved in oocyte nucleus migration, and thus the EGFR ligand, Gurken (Neuman-Silberberg and Schupbach, 1994).

6.2 Immunoassay:

Ovary collections and fixations were completed as previously described (Yakoby et al., 2008b). Primary antibodies: mouse anti-BR core (25E9.D7; 1:100, DSHB), rabbit anti-phosphorylated-Smad1/5/8 (1:3600, a gift from D. Vasiliauskas, S. Morton, T. Jessell and E. Laufer) (Yakoby et al., 2008b), Fasiclin III (FasIII – 1:100, DSHB), and DAPI (1:10,000). Secondary antibodies: 488 anti-mouse and 568 anti-rabbit (Invitrogen) were used (1:1000).

6.3 dpERK staining:

Ovaries for dpERK staining were dissected in ice cold graces medium during dissection. Due to the instability of dpERK, every pair of ovaries were immediately fixed in 80ul of PFA, 600ul of Heptane, and 120ul of 0.2% PBS Triton. After 10 minutes of dissection, samples were fixed for 20 minutes with a fresh fix solution. Fixed tissue was incubated for 1 min with protease K (Fisher) (1ul of 10mg/ml in 800ul of PBST), then immediately rinsed and washed 3 times for 5 minutes with 0.2% PBS Triton followed by a post fix of 4% PFA. Antibodies used were rabbit anti-dpERK (Cell Signaling) at 1:100, nucleus staining was done using mouse anti-Half-Pint (1:100) (Van Buskirk and Schupbach, 2002) and DAPI (1:10,000). *D. melanogaster* mouse anti-Gurken (1D12, Developmental Studies Hybridoma Bank – DSHB, IA) was used 1:10. In this project,

polyclonal Gurken antibodies (mouse) for *D. willistoni* (amino acids 88-243) and *D. cardini* (amino acids 1-255) were made by Primmbiotech (Cambridge, MA). Preabsorped antibodies were used at 1:100 as described (Yakoby et al., 2008b). Actin was stained using phalloidin (1:100) (Life Technologies).

6.4 Probe synthesis and *in situ* hybridization:

RNA extractions from the ovaries of all species were carried out using RNeasy Mini Kit (Qiagen). cDNA was synthesized using Taqman Kit (Roch). Primers for *tkv*, *Cp* genes, and *grk* amplification are located in chapter 6.12. PCR was done using the MJ Mini (BioRad) thermocycler and products were cloned using StrataClone PCR Cloning kit (Stratagene). Plasmids were recovered using the QIAprep spin Miniprep Kit (Qiagen). Each gene was sequenced (GeneWiz) and compared to known sequences on FlyBase. RNA DIG-labeled probes were synthesized and *in situ* hybridization was performed (Yakoby et al., 2008a). *In situ* hybridizations were carried out as described elsewhere (Wang et al., 2006; Yakoby et al., 2008b). *In situ* hybridization for *D. nebulosa grk* and *Cp* genes was carried out using *D. willistoni* probes.

6.5 Microscopy:

A Leica DM2500 compound microscope was used to image all egg chambers. In figure 23, stained egg chambers were imaged using a Leica SP5 confocal microscope (Imaging Core Facility, Princeton University, NJ). Images were processed with ImageJ (National Institutes of Health). SEM images were obtained as described in (Niepielko et al., 2014). The dorsal ridge was artificially colored using Photoshop (Adobe).

6.6 *D. willistoni grk* loci cloning:

Genomic DNA was isolated from *D. willistoni* (VDRC protocol). The *D. willistoni grk* loci was amplified using the Qiagen long range PCR kit and protocol with primers found in chapter 6.12. *D. willistoni grk* loci was topo cloned into pCR8 plasmid (Invitrogen). The pCR8 vector containing the *D. willistoni grk* loci was gateway cloned using LR reaction between a modified pBPGUw (pBw) (Pfeiffer et al., 2008) (Addgene 17575) vector and pCR8-*will-grk* with Invitogen LR II clonase. Modification of pBw included the exclusion of the Gal4, terminator, and promoter regions using *Fse*1 and *Xba*1, followed by ligation of the annealed primers CCCTAGCCCTGCAGGCT and CTAGAGCCTGGAGGGCTAGGGCCGG into the two restriction sites. pBw-*will-grk* was injected into *D. melanogaster* at position 68A4 of the attP2 fly (Genetic Services, MA).

6.7 Intensity profile:

Quantification of BMP signaling (assayed by monitoring P-MAD) gradient was carried out as was previously described (Vuilleumier et al., 2010). BMP signaling was measured by fluorescence-based imaging of the gradient of signaling activation that was determined by quantifying the levels of P-MAD. Specifically, we used a fixed rectangular box along the dorsal midline of the follicle cells, which was positioned from the anterior towards the posterior between the two Broad patches. The average pixel intensity was calculated as a function of distance from the anterior end using ImageJ *plot* profile function. The average value of seven independent egg chambers (n=7) is presented for the three conditions (WT, T155>*tkv,* CY2>*tkv*). The plot profiles data were exported to Microsoft Excel, and graphs were generated using 17 pixels per cell. Specifically, the

transformation of pixels into the number of cells was done by taking the average pixel length of the follicle cells (~425), and dividing it by the average number of follicle cells (~25) from the anterior border of the oocyte to the posterior end of stage 10 egg chambers (17 pixels per cell).

To accurately compare distances of P-MAD signaling among the three conditions, the plot profiles data were normalized for all 21 measurements by dividing the highest intensity into all intensities. The average percent intensity of each condition and the standard errors were plotted starting with the highest intensity. The P-MAD gradients were fit to an exponential gradient in MATLAB using the command *fit*. The significance of the difference in the λ values between different backgrounds was tested using Student's t-test. The MATLAB command *ttest2* was used for this purpose.

6.8 Computational modeling:

The mathematical model is based on previous work done to simulate BMP signaling activation in the follicle cells (FCs) of *D. melanogaster* (Lembong et al., 2008). The system was modeled over a half prolate spheroidal grid. Ligand diffusion was simulated within the perivitelline space (PVS) (Cavaliere et al., 2008) emanating uniformly from an anterior boundary followed by its binding and internalization by receptors. Signaling activation was assumed to linearly follow receptor-ligand internalization. Here, the model was extended to simulate the activation of BMP signaling in different receptor expression patterns. These patterns reflect the expression of *tkv* in different species. We used a dimensionless parameter (φ) to describe the diffusion length of the ligand in the presence of a receptor. The specific φ values are described in the text and were deduced from an exponential curve fitted to the

experimentally measured signaling gradients. Solutions for the morphogen concentration M were obtained by using second-order finite difference methods to discretize the problem before solving numerically in MATLAB (MathWorks, Natick MA). Computational solutions were projected onto two-dimensions for presentation purposes.

6.9 Matrices and matrix analysis:

Gene patterns are represented as binary vectors consisting of mutually exclusive domains at four different developmental stages of *Drosophila* oogenesis (Spradling, 1993; Yakoby et al., 2008a). In the original combinatorial code (Yakoby et al., 2008a), the anterior, dorsal and midline domains overlap. Here, we modified them to be mutually exclusive. The anterior domain was split into anterior-dorsal (AD) and anterior-ventral (AV) domains and a domain for dorsal ridge (DR) and posterior (P) were added as well as repression domains (for the complete details see Fig. 17). Representation and manipulation of matrices were conducted with MATLAB (The MathWorks, Natick, MA) and displayed using the *imagesc* command. Hierarchical clustering was conducted (Eisen et al., 1998) on an averaged expression matrix of all three species in order to determine expression domain relatedness. Bootstrap values were calculated by assembling a UPGMA tree in Mega5 (Tamura et al., 2011) with 1000 bootstrap trees, representing domain conservation with individual nucleotides. Distance was determined with the Euclidean distance metric and average linkage was used for tree generation. Clustergrams are generated such that genes cluster on one axis and domains cluster on the other.

6.10 RNAi constructs and injection:

Short hairpin RNAi against *grk* were designed as described (Haley et al., 2008) and were checked for possible off targets using BLAST searches. Oligos for the top and bottom strands of *D. willistoni* and *D. melanogaster* RNAi strands are found in chapter 6.12. Only two bases differ between *D. melanogaser* and *D. willistoni* (denoted in Fig. 24). Oligos were designed to ligate into *Fse*1 and *Not*1 cut sites. Annealed strands were ligated into *Not*1 and *Fse*1(Bio Labs) restricted UASpBacNPF vector (Holtzman et al., 2010) and electroporated into DH5α. Vectors containing RNAi constructs were recovered using the Qiagen midi prep kit and sequenced (Genewiz, NJ). Plasmids were injected into w^- *D. melanogaster* (Genetic Services, MA) and pBac-Blue-eyed *D. willistoni* (Rainbow Transgenics, CA) as previously described (Holtzman et al., 2010).

6.11 Heat shock treatments:

Gurken RNAi was expressed with heat shock treatments, 1 hour at 37C three times a day (the transformation vector contains a minimal heat shock promoter (Holtzman et al., 2010).

6.12 Oligonucleotides:

Species_GENE_Direction	**PRIMER SEQUENCE**
Dgenerate_*tkv_5'*	AGYAAYGGHACCTGCGAGAC
Dgenerate_*tkv_3'*	GYGKATTCTGYGCAATGTGRAT
*D. mel*_Cp15_5'	CCCTTTTCGCCTACATCAAC
*D. mel*_Cp15_3'	ATTGCGTTCAAGCTGCTTTT
*D. wil*_Cp15_5'	CTGTTCGTTTGCATCAGCTT
*D. wil*_Cp15_3'	TTGTATCCACCATCGATCTCC

*D. mel*_Cp16_5'	CAAGCTCTTAGATGGCCACA
*D. mel*_Cp16_3'	GCATAGAAATTGGAGACGATCC
*D. wil*_Cp16_5'	GCACCACCATAGTGGCTCTT
*D. wil*_Cp16_3'	GTCAAGCCCTACGAGACAGC
*D. mel*_Cp18_5'	TCGCATCGATCAACTAACCA
*D. mel*_Cp18_3'	GGCCTCTTGTAGCCCTTCTT
*D. wil*_Cp_18_5'	TGCTGTTTCTGCCTATGGTG
*D. wil*_Cp_18_3'	TAGCCGGACTTCTTGTAGCC
*D. mel*_Cp_19_5'	CAACTGTGCCAAAACCCATA
*D. mel*_Cp_19_3'	CACGATCAGGCTGAGATCAA
*D. wil*_Cp_19_5'	ATTCATCTGCGCCTATCTGG
*D. wil*_Cp_19_3'	TATTTGGGTCCCTCAACACC
*D. mel*_Cp_36_5'	ATGCAACTCGGTCTCTGGTT
*D. mel*_Cp_36_3'	TGTACAGTGGAGCCTCGTTG
*D. wil*_Cp_36_5'	GTCTCTGGTTTGGGCTTTTC
*D. wil*_Cp_36_3'	AGTAGTTCTGCTGGCCATAGG
*D. mel*_Cp_38_5'	TGCAACTGGGAGACAAGATG
*D. mel*_Cp_38_3'	GCCGGATAAGCGAATGACTA
*D. wil*_Cp_38_5'	CCTGCCTGATTGCATGTG
*D. wil*_Cp_38_3'	AATATGCAGGAGCGCCATAG
*D. mel*_Cp_7fa_5'	CTTCTTCTCGCGTTGGTCAT
*D. mel*_Cp_7fa_3'	ATTGGAATTGGATTGGATGG
*D. wil*_Cp_7fa_5'	GTCAGTGTGCAAGGGCTTCT
*D. wil*_Cp_7fa_3'	CAATAACAATTGCCCGCATC

*D. mel*_Cp_7fb_5'	GAGGAGCAAGTGCCTCAAAC
*D. mel*_Cp_7fb_3'	GTTGCATTCGGTTTGGAGTT
*D. wil*_7fb_5'	TTGCTCGAGCTGTTCGTCTA
*D. wil*_7fb_3'	GATCGACAAGATCGCCAAAT
*D. mel*_7fc_5'	CCCCGATGAGGAATACAATG
*D. mel*_7fc_3'	TCTGGAGACCGCAAGTCTTT
*D. wil*_7fc_5'	CCAATTGGTGGCTATTGTTAC
*D. wil*_7fc_3'	TCCTCGCCTGTAGAGTAAATAGG
mel/card-gurken-fwd	TTGTCKCMGTCACAGATTG
mel/card-gurken-rev	CGHTGCTTRTGCARRTGYA
will-grk-fwd	CGGGAACATACGCTGAAAAT
will-grk-rev	ATCGGCACACACACATGAAT
will-grk-loci-fwd	GCCCGTTACATGCGAATAAT
will-grk-loc-rev	GAGCCACAAACGTAGCATCA

***Gurken* RNAi oligos**

will-sh*grk*-RNAi-top strand

GGCCGCAGTAATTGTGCAGGATCAGCATTATAGTTATATTCAAGCATATTATG
CTGATGCTGCACAATTGCGGCCGG

will-sh*grk*-RNAi-bottom strand

CCGCAATTGTGCAGCATCAGCATAATATGCTTGAATATAACTATAATGCTGAT
CCTGCACAATTACTGC

mel-sh*grk*-RNAi-top strand

GGCCGCAGTAATTGTGCAGGATCAGCACTGTAGTTATATTCAAGCATACTGT
GCTGATGCTGCACAATTGCGGCCGG

mel-sh*grk*-RNAi-bottom strand

CCGCAATTGTGCAGCATCAGCACAGTATGCTTGAATATAACTACAGTGCTGA
TCCTGCACAATTACTGC

Chapter 7: Supplemental Material

Supp 1A- Cp7fa

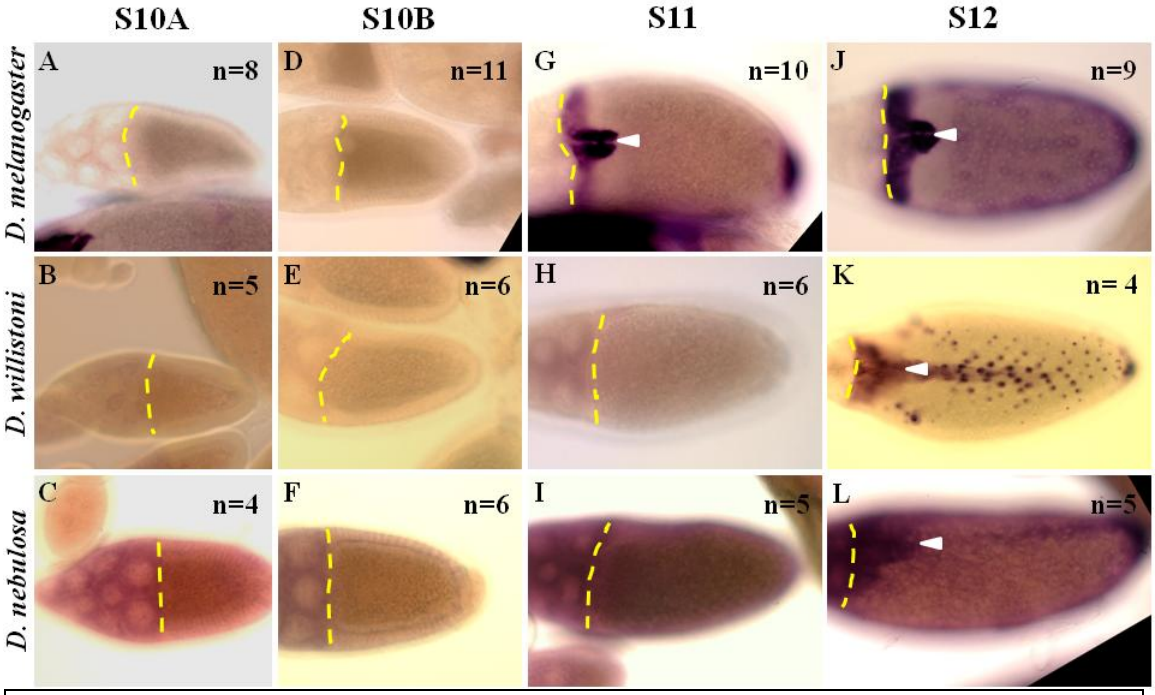

Supp 1A: Patterning dynamics of Cp7fa in *D. melanogaster, D. willistoni* and *D. nebulosa*. Top Row: *D. melanogaster*. Middle Row: *D. willistoni*. Bottom Row: *D. nebulosa*. (A-C) Stage 10A, (D-F) Stage 10B, (G-I) Stage 11, and (J-L) Stage 12. Broken yellow line marks the anterior most follicle cells and white arrowhead denotes dorsal midline. Numbers (n) denote the count of similar patterns to the one presented in the figure.

Supp 1B- Cp7fb

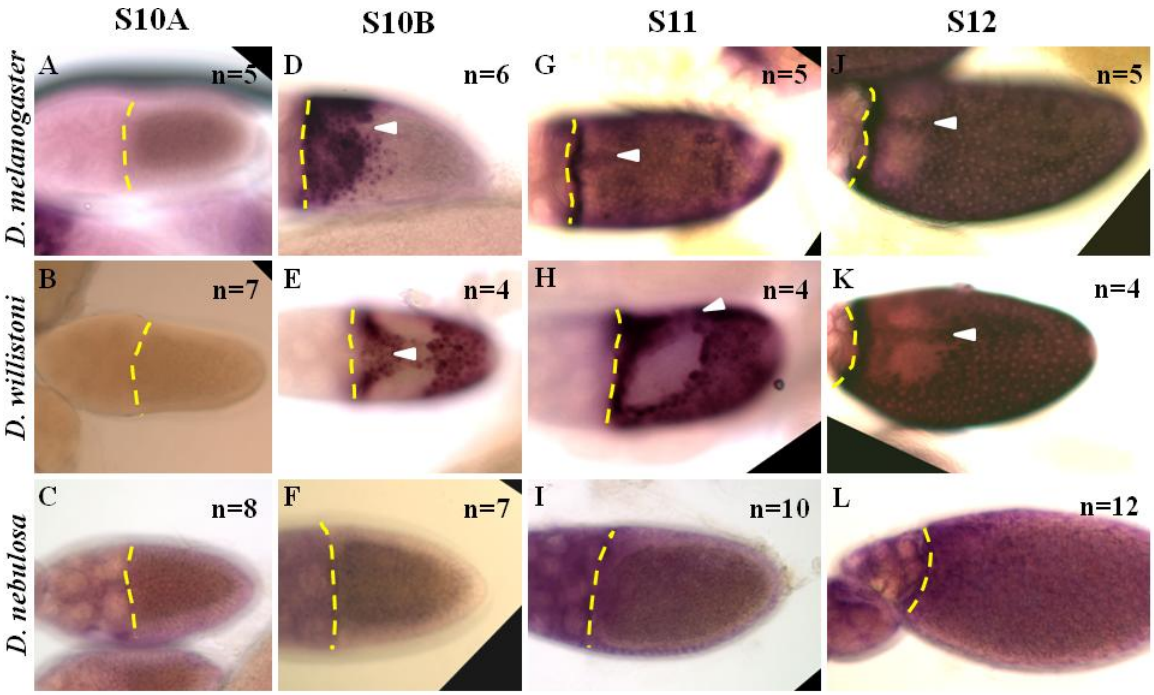

Supp 1B: Patterning dynamics of Cp7fb in *D. melanogaster, D. willistoni* and *D. nebulosa*. Top Row: *D. melanogaster*. Middle Row: *D. willistoni*. Bottom Row: *D. nebulosa*. (A-C) Stage 10A, (D-F) Stage 10B, (G-I) Stage 11, and (J-L) Stage 12. Broken yellow line marks the anterior most follicle cells and white arrowhead denotes dorsal midline. Numbers (n) denote the count of similar patterns to the one presented in the figure.

Supp 1C- Cp7fc

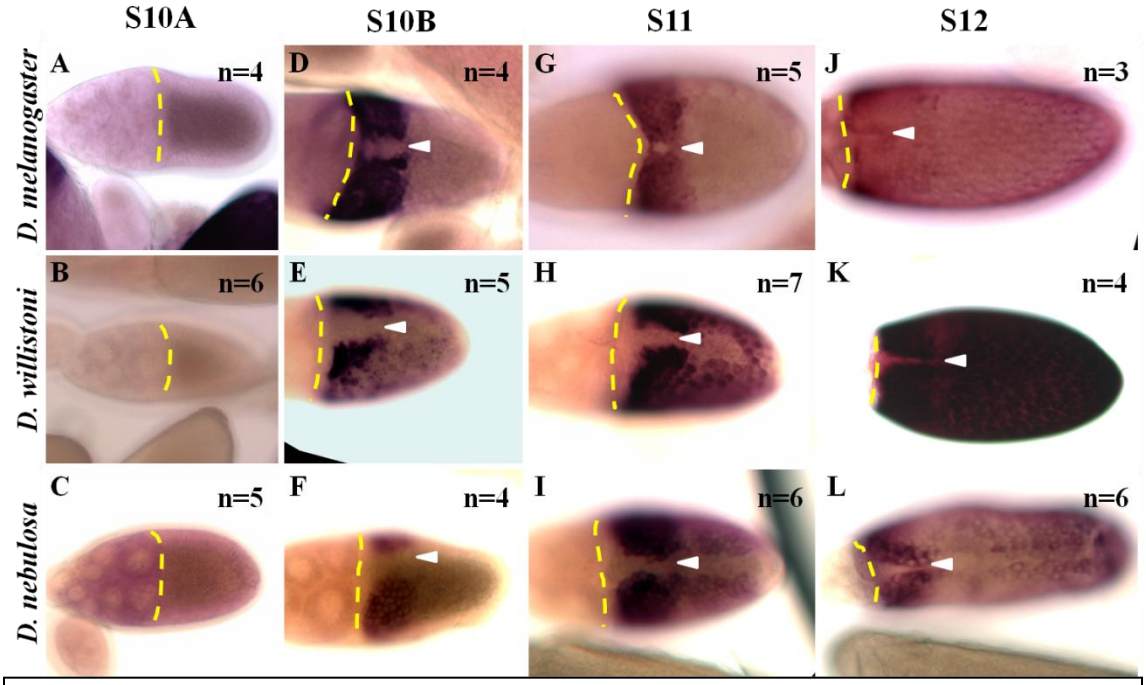

Supp 1C: Patterning dynamics of Cp7fc in *D. melanogaster, D. willistoni* and *D. nebulosa*. Top Row: *D. melanogaster*. Middle Row: *D. willistoni*. Bottom Row: *D. nebulosa*. (A-C) Stage 10A, (D-F) Stage 10B, (G-I) Stage 11, and (J-L) Stage 12. Broken yellow line marks the anterior most follicle cells and white arrowhead denotes dorsal midline. Numbers (n) denote the count of similar patterns to the one presented in the figure.

Supp 1D- Cp15

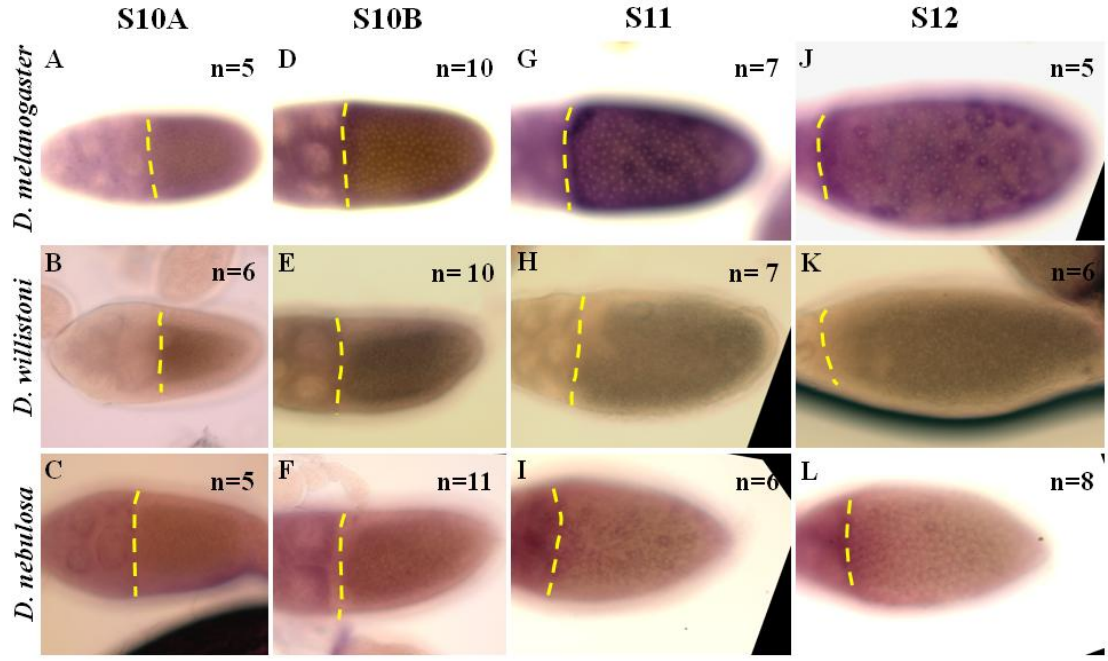

Supp 1D: Patterning dynamics of Cp15 in *D. melanogaster, D. willistoni* and *D. nebulosa*. Top Row: *D. melanogaster*. Middle Row: *D. willistoni*. Bottom Row: *D. nebulosa*. (A-C) Stage 10A, (D-F) Stage 10B, (G-I) Stage 11, and (J-L) Stage 12. Broken yellow line marks the anterior most follicle cells and white arrowhead denotes dorsal midline. Numbers (n) denote the count of similar patterns to the one presented in the figure.

Supp 1E- Cp16

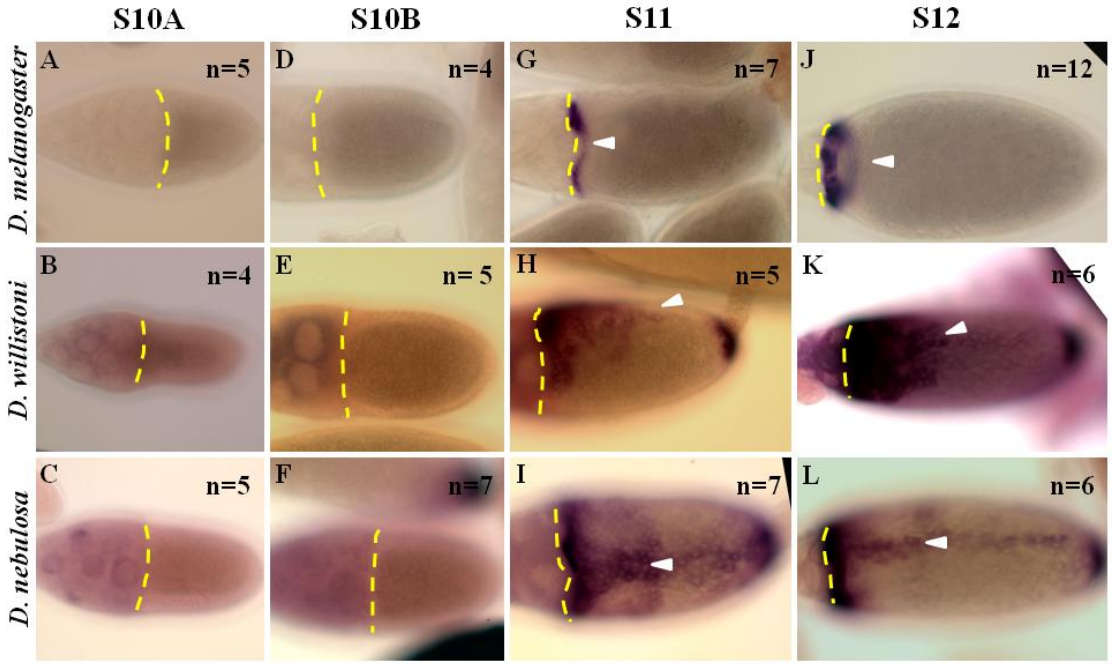

Supp 1E: Patterning dynamics of Cp16 in *D. melanogaster, D. willistoni* and *D. nebulosa*. Top Row: *D. melanogaster*. Middle Row: *D. willistoni*. Bottom Row: *D. nebulosa*. (A-C) Stage 10A, (D-F) Stage 10B, (G-I) Stage 11, and (J-L) Stage 12. Broken yellow line marks the anterior most follicle cells and white arrowhead denotes dorsal midline. Numbers (n) denote the count of similar patterns to the one presented in the figure.

Supp 1F- Cp18

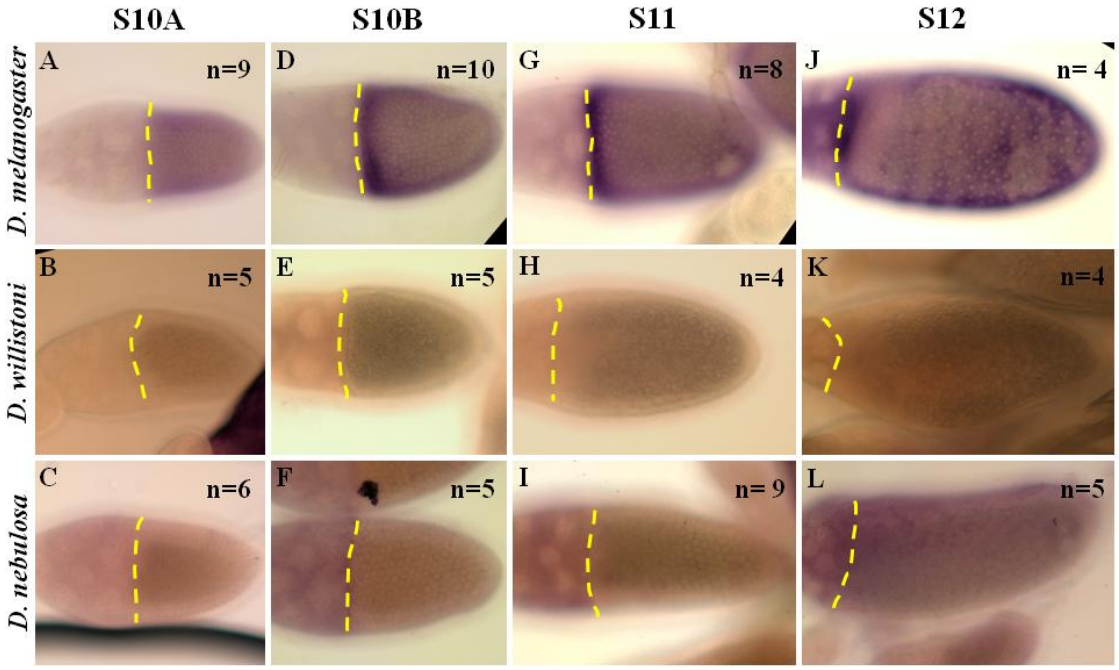

Supp 1F: Patterning dynamics of Cp18 in *D. melanogaster, D. willistoni* and *D. nebulosa*. Top Row: *D. melanogaster*. Middle Row: *D. willistoni*. Bottom Row: *D. nebulosa*. (A-C) Stage 10A, (D-F) Stage 10B, (G-I) Stage 11, and (J-L) Stage 12. Broken yellow line marks the anterior most follicle cells and white arrowhead denotes dorsal midline. Numbers (n) denote the count of similar patterns to the one presented in the figure.

Supp 1G- Cp19

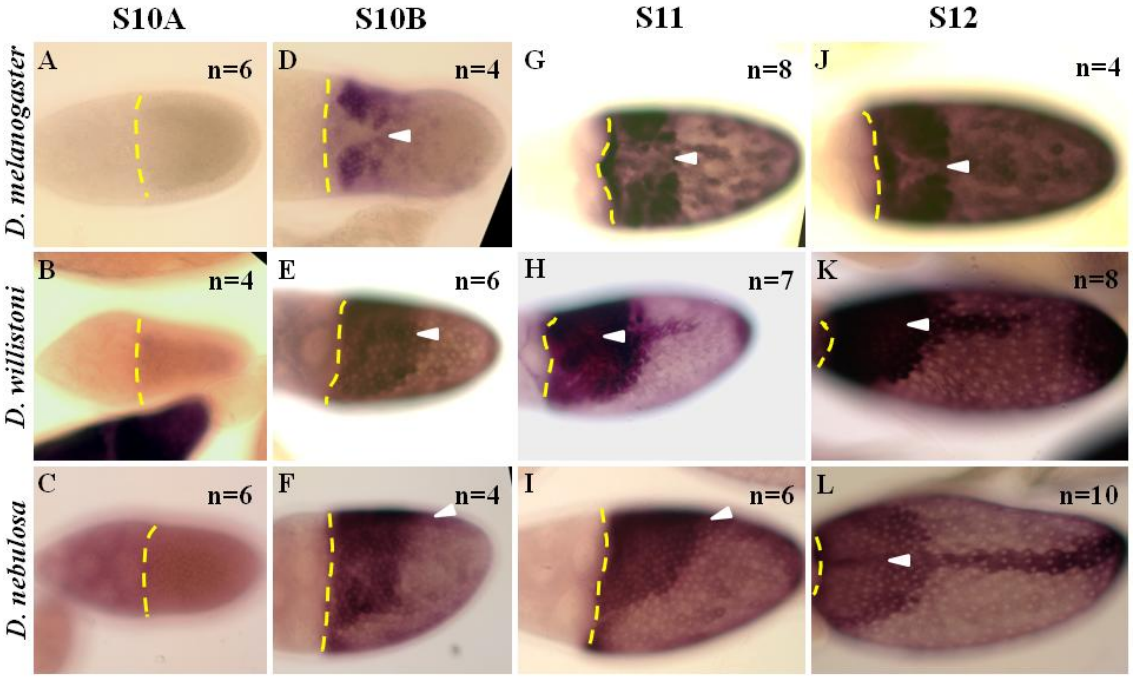

Supp 1G: Patterning dynamics of Cp19 in *D. melanogaster*, *D. willistoni* and *D. nebulosa*. Top Row: *D. melanogaster*. Middle Row: *D. willistoni*. Bottom Row: *D. nebulosa*. (A-C) Stage 10A, (D-F) Stage 10B, (G-I) Stage 11, and (J-L) Stage 12. Broken yellow line marks the anterior most follicle cells and white arrowhead denotes dorsal midline. Numbers (n) denote the count of similar patterns to the one presented in the figure.

Supp 1H- Cp36

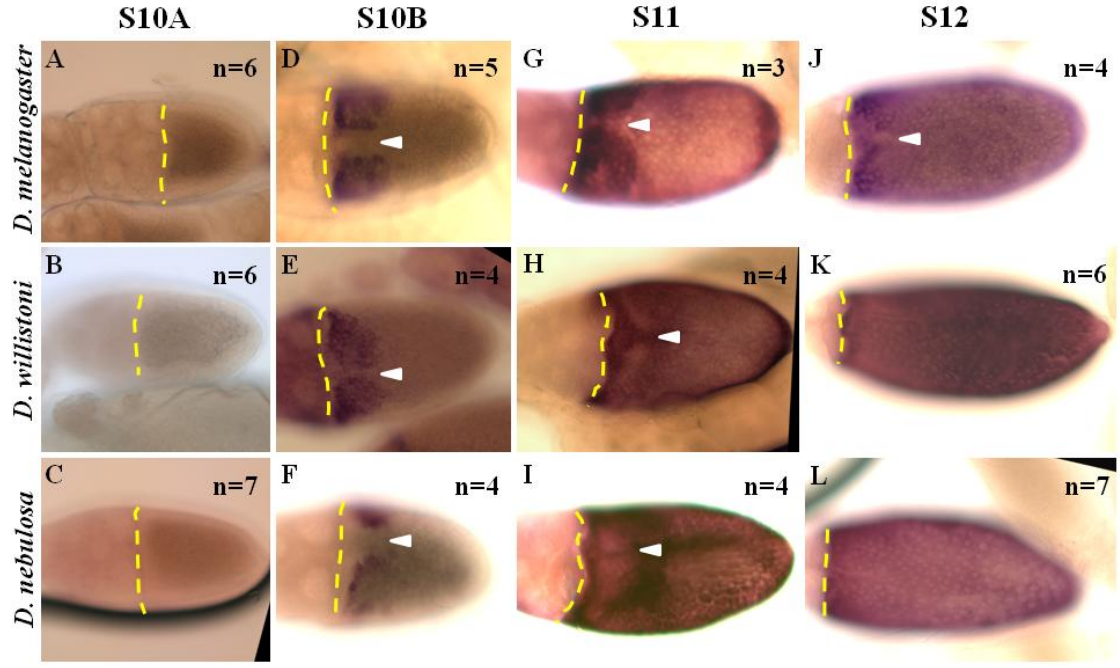

Supp 1H: Patterning dynamics of Cp36 in *D. melanogaster*, *D. willistoni* and *D. nebulosa*. Top Row: *D. melanogaster*. Middle Row: *D. willistoni*. Bottom Row: *D. nebulosa*. (A-C) Stage 10A, (D-F) Stage 10B, (G-I) Stage 11, and (J-L) Stage 12. Broken yellow line marks the anterior most follicle cells and white arrowhead denotes dorsal midline. Numbers (n) denote the count of similar patterns to the one presented in the figure.

Supp 1I- Cp38

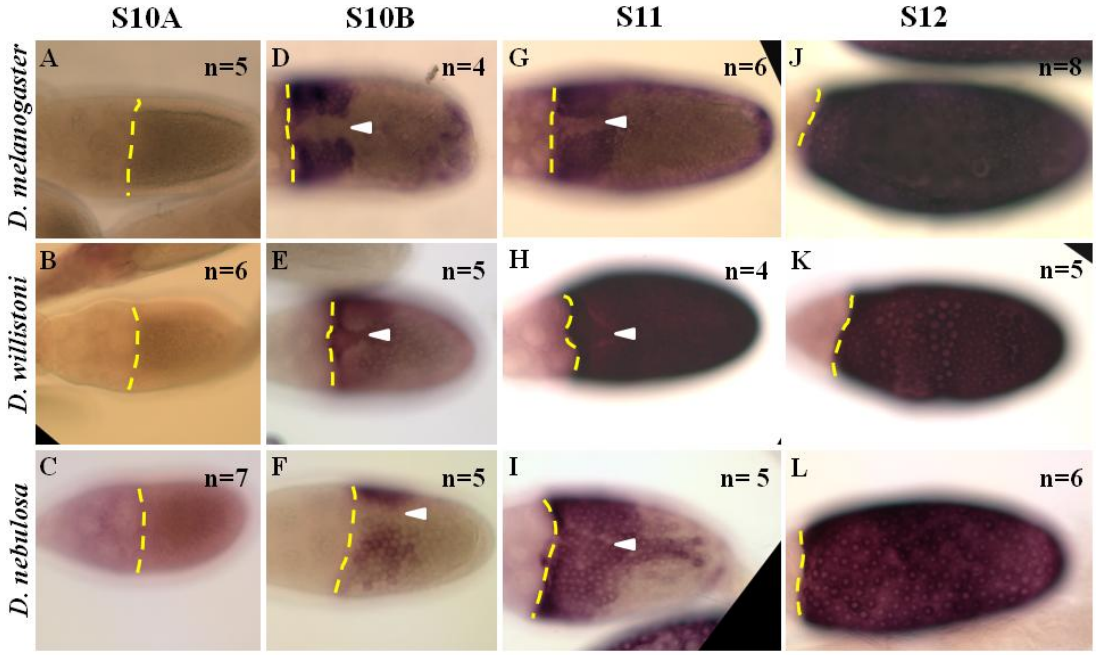

Supp 1I: Patterning dynamics of Cp38 in *D. melanogaster*, *D. willistoni* and *D. nebulosa*. Top Row: *D. melanogaster*. Middle Row: *D. willistoni*. Bottom Row: *D. nebulosa*. (A-C) Stage 10A, (D-F) Stage 10B, (G-I) Stage 11, and (J-L) Stage 12. Broken yellow line marks the anterior most follicle cells and white arrowhead denotes dorsal midline. Numbers (n) denote the count of similar patterns to the one presented in the figure.

Supp 2A: Colchicine +

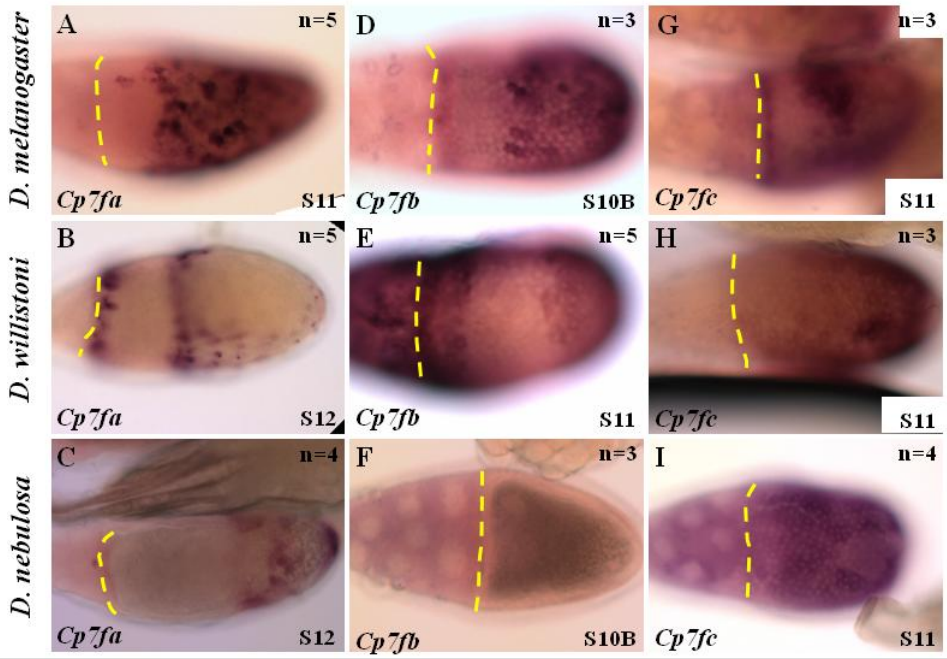

Supp 2A: Supplement Figure 3A: Colchicine affected egg chamber with patterns of Cp7fa, Cp7fb, and Cp7fc. *D. melanogaster* (A, D, G). *D. willistoni* (B, E, F). *D. nebulosa* (C, F, I). (A-C) Cp7fa, (D-F) Cp7fb, and (G-I) Cp7fc. Broken yellow line marks the anterior most follicle cells.

Supp 2B: Colchicine +

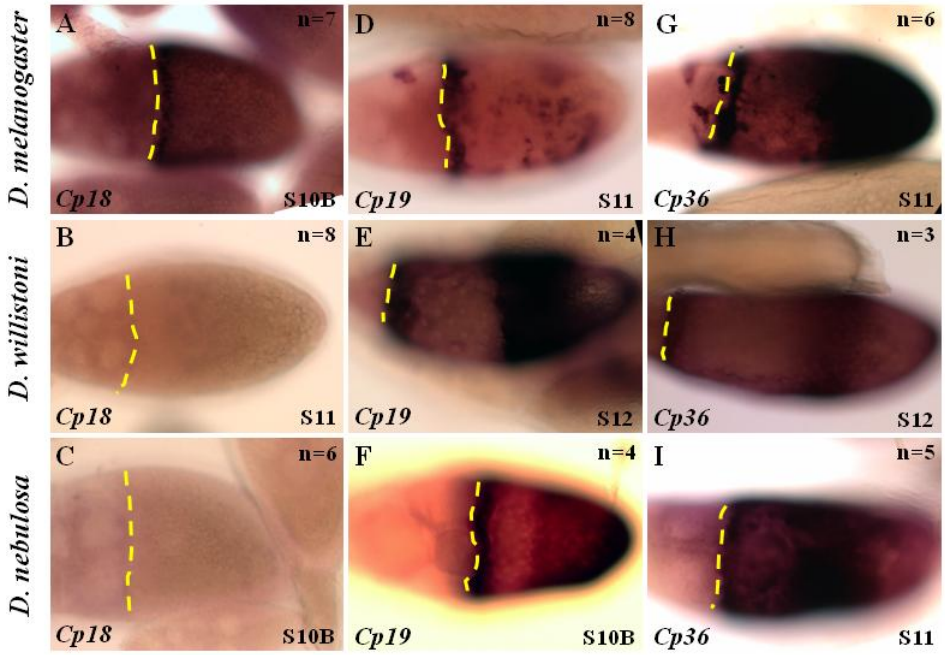

Supp 2B: Colchicine affected egg chamber with patterns of Cp18, Cp19, and Cp36. *D. melanogaster* (A, D, G). *D. willistoni* (B, E, H). *D. nebulosa* (C, F, I). (A-C) Cp18, (D-F) Cp19, and (G-I) Cp36. Broken yellow line marks the anterior most follicle cells.

Supp 2C: Colchicine +

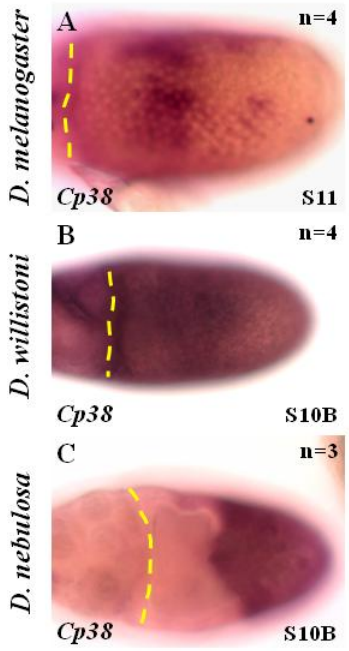

Supp 2C: Colchicine affected egg chamber with patterns of Cp38. *D. melanogaster* (A). *D. willistoni* (B). *D. nebulosa* (C). Broken yellow line marks the anterior most follicle cells.

Supp 3A

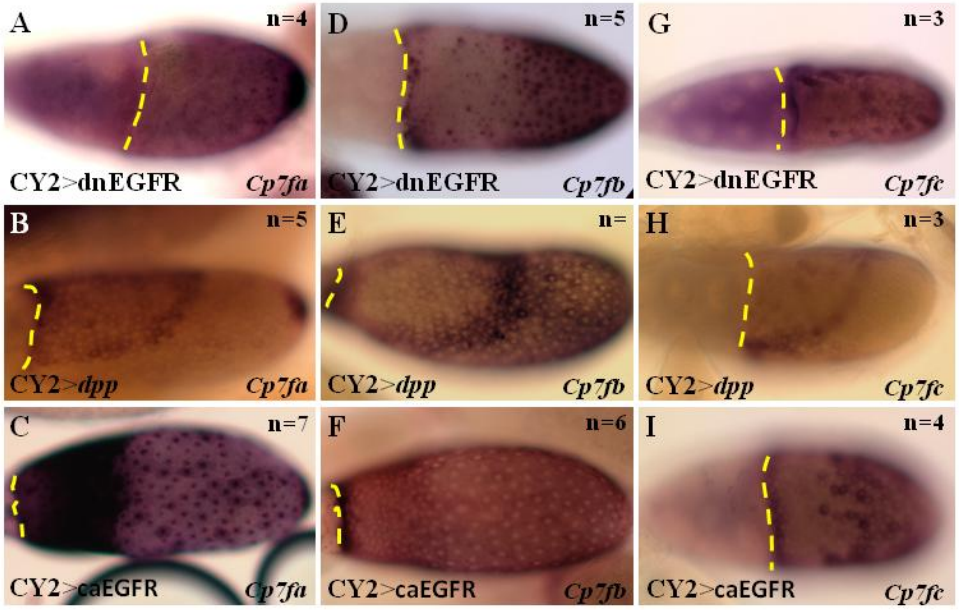

Supp 3A: Genetically perturbed egg chamber with patterns of Cp7fa, Cp7fb, and Cp7fc. CY2>dnEGFR (A, D, G). CY2>dpp (B, E, H). CY2>caEGFR (C, F, I). (A-C) Cp7fa, (D-F) Cp7fb, and (G-I) Cp7fc. Broken yellow line marks the anterior most follicle cells.

Supp 3B

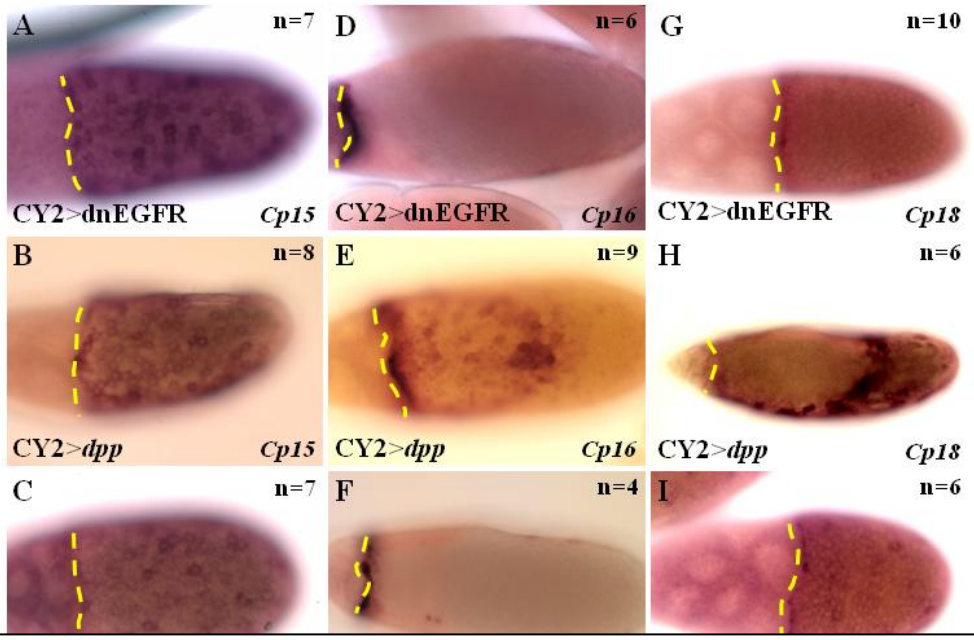

Supp 3B: Genetically perturbed egg chamber with patterns of Cp15, Cp16, and Cp18. CY2>dnEGFR (A, D, G). CY2>dpp (B, E, H). CY2>caEGFR (C, F, I). (A-C) Cp15, (D-F) Cp16, and (G-I) Cp18. Broken yellow line marks the anterior most follicle cells.

Supp 3C

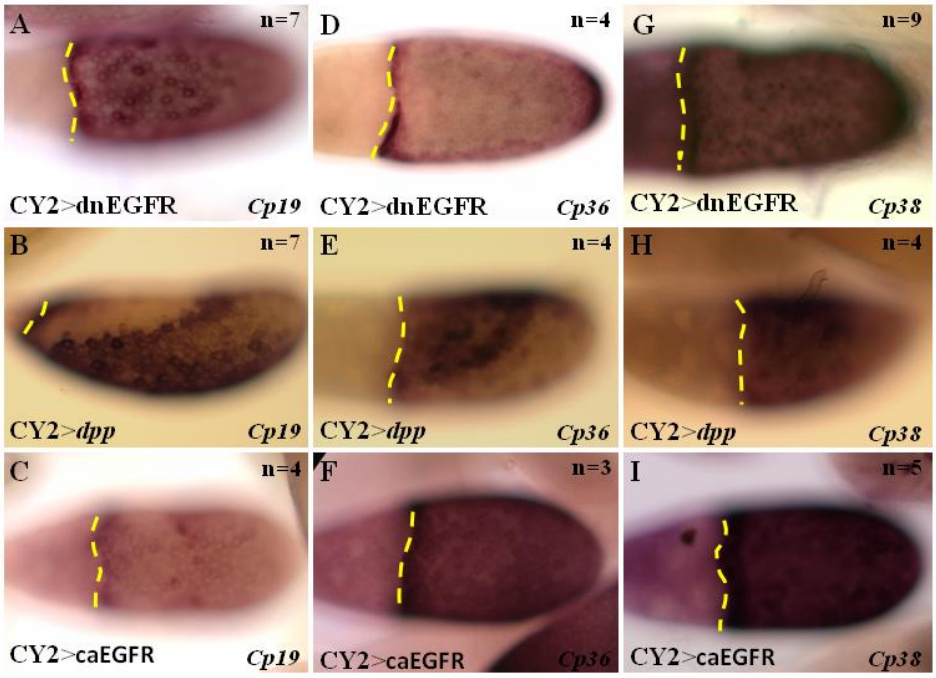

Supp 3C: Genetically perturbed egg chamber with patterns of Cp19, Cp36, and Cp38. CY2>dnEGFR (A, D, G). CY2>dpp (B, E, H). CY2>caEGFR (C, F, I). (A-C) Cp19, (D-F) Cp36, and (G-I) Cp38. Broken yellow line marks the anterior most follicle cells.

8: References

Abzhanov, A., Protas, M., Grant, B.R., Grant, P.R., Tabin, C.J., 2004. Bmp4 and morphological variation of beaks in Darwin's finches. Science 305, 1462-1465.

Affolter, M., Basler, K., 2007. The Decapentaplegic morphogen gradient: from pattern formation to growth regulation. Nat Rev Genet 8, 663-674.

Ashe, H.L., Briscoe, J., 2006. The interpretation of morphogen gradients. Development 133, 385-394.

Ashe, H.L., Levine, M., 1999. Local inhibition and long-range enhancement of Dpp signal transduction by Sog. Nature 398, 427-431.

Berg, C.A., 2005. The Drosophila shell game: patterning genes and morphological change. Trends in genetics : TIG 21, 346-355.

Berg, C.A., 2008. Tube formation in Drosophila egg chambers. Tissue Eng Part A 14, 1479-1488.
Boisclair Lachance, J.F., Fregoso Lomas, M., Eleiche, A., Bouchard Kerr, P., Nilson, L.A., 2009. Graded Egfr activity patterns the Drosophila eggshell independently of autocrine feedback. Development 136, 2893-2902.

Carroll, S.B., 2005. Evolution at two levels: on genes and form. PLoS Biol 3, e245.

Carroll, S.B., 2008. Evo-devo and an expanding evolutionary synthesis: a genetic theory of morphological evolution. Cell 134, 25-36.

Cavaliere, V., Bernardi, F., Romani, P., Duchi, S., Gargiulo, G., 2008. Building up the Drosophila eggshell: first of all the eggshell genes must be transcribed. Dev Dyn 237, 2061-2072.

Chen, Y., Schupbach, T., 2006. The role of brinker in eggshell patterning. Mechanisms of development 123, 395-406.

Crickmore, M.A., Mann, R.S., 2006. Hox control of organ size by regulation of morphogen production and mobility. Science 313, 63-68.

Davidson, E.H., Erwin, D.H., 2006. Gene regulatory networks and the evolution of animal body plans. Science 311, 796-800.

De Robertis, E.M., 2008. Evo-Devo: Variation on ancestral themes. Cell 132, 185-195.

Deng, W.M., Bownes, M., 1997. Two signalling pathways specify localised expression of the Broad-Complex in Drosophila eggshell patterning and morphogenesis. Development 124, 4639-4647.

Dequier, E., Souid, S., Pal, M., Maroy, P., Lepesant, J.A., Yanicostas, C., 2001. Top-DER- and Dpp-dependent requirements for the Drosophila fos/kayak gene in follicular epithelium morphogenesis. Mechanisms of development 106, 47-60.

Dobens, L.L., Hsu, T., Twombly, V., Gelbart, W.M., Raftery, L.A., Kafatos, F.C., 1997. The Drosophila bunched gene is a homologue of the growth factor stimulated mammalian TSC-22 sequence and is required during oogenesis. Mechanisms of development 65, 197-208.
Dobens, L.L., Raftery, L.A., 1998. Drosophila oogenesis: a model system to understand TGF-beta/Dpp directed cell morphogenesis. Ann N Y Acad Sci 857, 245-247.

Dobens, L.L., Raftery, L.A., 2000. Integration of epithelial patterning and morphogenesis in Drosophila ovarian follicle cells. Dev Dyn 218, 80-93.

Dong, X., Tsuda, L., Zavitz, K.H., Lin, M., Li, S., Carthew, R.W., Zipursky, S.L., 1999. ebi regulates epidermal growth factor receptor signaling pathways in Drosophila. Genes & development 13, 954-965.

Dorman, J.B., James, K.E., Fraser, S.E., Kiehart, D.P., Berg, C.A., 2004. bullwinkle is required for epithelial morphogenesis during Drosophila oogenesis. Dev Biol 267, 320-341.

Eisen, M.B., Spellman, P.T., Brown, P.O., Botstein, D., 1998. Cluster analysis and display of genome-wide expression patterns. Proceedings of the National Academy of Sciences of the United States of America 95, 14863-14868.

Eldar, A., Dorfman, R., Weiss, D., Ashe, H., Shilo, B.Z., Barkai, N., 2002. Robustness of the BMP morphogen gradient in Drosophila embryonic patterning. Nature 419, 304-308.

Fakhouri, M., Elalayli, M., Sherling, D., Hall, J.D., Miller, E., Sun, X., Wells, L., LeMosy, E.K., 2006. Minor proteins and enzymes of the Drosophila eggshell matrix. Dev Biol 293, 127-141.

Fuentealba, L.C., Eivers, E., Ikeda, A., Hurtado, C., Kuroda, H., Pera, E.M., De Robertis, E.M., 2007. Integrating patterning signals: Wnt/GSK3 regulates the duration of the BMP/Smad1 signal. Cell 131, 980-993.

Goentoro, L.A., Reeves, G.T., Kowal, C.P., Martinelli, L., Schupbach, T., Shvartsman, S.Y., 2006. Quantifying the Gurken morphogen gradient in Drosophila oogenesis. Dev Cell 11, 263-272.

Goltsev, Y., Fuse, N., Frasch, M., Zinzen, R.P., Lanzaro, G., Levine, M., 2007. Evolution of the dorsal-ventral patterning network in the mosquito, Anopheles gambiae. Development 134, 2415-2424.

Gordon, K.L., Ruvinsky, I., 2012. Tempo and mode in evolution of transcriptional regulation. PLoS Genet 8, e1002432.

Griffin-Shea, R., Thireos, G., Kafatos, F.C., 1982. Organization of a cluster of four chorion genes in Drosophila and its relationship to developmental expression and amplification. Dev Biol 91, 325-336.

Haley, B., Hendrix, D.A., Trang, V., Levine, M., 2008. A simplified miRNA-based gene silencing method for *Drosophila melanogaster*. Dev Biol 15, 282-290.

Hinton, H.E., 1981. Biology of insect eggs. Pergamon Press, Oxford.

Holtzman, S., Miller, D., Eisman, C.R., Kuwayama, H., Niimi, T., Kaufman, T.C., 2010. Transgenic tools for members of the genus Drosophila with sequenced genomes. Fly 4, 1-14.

Horne-Badovinac, S., Bilder, D., 2005. Mass transit: epithelial morphogenesis in the Drosophila egg chamber. Dev Dyn 232, 559-574.

Jekely, G., Rorth, P., 2003. Hrs mediates downregulation of multiple signalling receptors in Drosophila. EMBO Rep 4, 1163-1168.

Kagesawa, T., Nakamura, Y., Nishikawa, M., Akiyama, Y., Kajiwara, M., Matsuno, K., 2008. Distinct activation patterns of EGF receptor signaling in the homoplastic evolution of eggshell morphology in genus Drosophila. Mech Dev 125, 1020-1032.

King, C.R., 1970. Ovarian Development in Drosophila melanogaster. Academic Press, London.
Lecuit, T., Brook, W.J., Ng, M., Calleja, M., Sun, H., Cohen, S.M., 1996. Two distinct mechanisms for long-range patterning by Decapentaplegic in the Drosophila wing. Nature 381, 387-393.

Lecuit, T., Cohen, S.M., 1998. Dpp receptor levels contribute to shaping the Dpp morphogen gradient in the Drosophila wing imaginal disc. Development 125, 4901-4907.

Lembong, J., Yakoby, N., Shvartsman, S.Y., 2008. Spatial regulation of BMP signaling by patterned receptor expression. Tissue Eng Part A 14, 1469-1477.

Lembong, J., Yakoby, N., Shvartsman, S.Y., 2009. Pattern formation by dynamically interacting network motifs. Proceedings of the National Academy of Sciences of the United States of America, 3213-3218.

Lynch, J.A., Peel, A.D., Drechsler, A., Averof, M., Roth, S., 2010. EGF signaling and the origin of axial polarity among the insects. Curr Biol 20, 1042-1047.

Mantrova, E.Y., Schulz, R.A., Hsu, T., 1999. Oogenic function of the myogenic factor D-MEF2: negative regulation of the decapentaplegic receptor gene thick veins. Proceedings of the National Academy of Sciences of the United States of America 96, 11889-11894.

Mao, Y., Freeman, M., 2009. Fasciclin 2, the Drosophila orthologue of neural cell-adhesion molecule, inhibits EGF receptor signalling. Development 136, 473-481.

Margaritis, L.H., Dellas, K., Kalantzi, M.C., Kambysellis, M.P., 1983. The eggshell of Hawaiian *Drosophila*: structural and biochemical studies in *D. grimshawi* and comparison to *D. melanogaster*. Roux's Archives of Developmental Biology, 303-316.

Margaritis, L.H., Kafatos, F.C., Petri, W.H., 1980. The eggshell of Drosophila melanogaster. I. Fine structure of the layers and regions of the wild-type eggshell. J Cell Sci 43, 1-35.

Massague, J., Blain, S.W., Lo, R.S., 2000. TGFbeta signaling in growth control, cancer, and heritable disorders. Cell 103, 295-309.

Massague, J., Gomis, R.R., 2006. The logic of TGFbeta signaling. FEBS letters 580, 2811-2820.
Mitsudomi, T., Yatabe, Y., 2010. Epidermal growth factor receptor in relation to tumor development: EGFR gene and cancer. The FEBS journal 277, 301-308.

Muller, P., Rogers, K.W., Yu, S.R., Brand, M., Schier, A.F., 2013. Morphogen transport. Development 140, 1621-1638.

Nakamura, Y., Kagesawa, T., Nishikawa, M., Hayashi, Y., Kobayashi, S., Niimi, T., Matsuno, K., 2007. Soma-dependent modulations contribute to divergence of rhomboid expression during evolution of Drosophila eggshell morphology. Development 134, 1529-1537.

Nakamura, Y., Matsuno, K., 2003. Species-specific activation of EGF receptor signaling underlies evolutionary diversity in the dorsal appendage number of the genus Drosophila eggshells. Mechanisms of development 120, 897-907.

Neuman-Silberberg, F.S., Schupbach, T., 1993. The Drosophila dorsoventral patterning gene gurken produces a dorsally localized RNA and encodes a TGF alpha-like protein. Cell 75, 165-174.

Neuman-Silberberg, F.S., Schupbach, T., 1994. Dorsoventral axis formation in Drosophila depends on the correct dosage of the gene gurken. Development 120, 2457-2463.

Neuman-Silberberg, F.S., Schupbach, T., 1996. The Drosophila TGF-alpha-like protein Gurken: expression and cellular localization during Drosophila oogenesis. Mechanisms of development 59, 105-113.

Niepielko, M.G., Hernaiz-Hernandez, Y., Yakoby, N., 2011. BMP signaling dynamics in the follicle cells of multiple Drosophila species. Dev Biol 354, 151-159.

Niepielko, M.G., Ip, K., Kanodia, J.S., Lun, D.S., Yakoby, N., 2012. The evolution of BMP signaling in *Drosophila* oogenesis: a receptor-based mechanism. Biophysical Journal 102, 1722-1730.

Niepielko, M.G., Marmion, R.A., Kim, K., Luor, D., Ray, C., Yakoby, N., 2014. Chorion Patterning: A Window into Gene Regulation and Drosophila Species' Relatedness. Mol Biol Evol 31, 154-164.

O'Connor, M.B., Umulis, D., Othmer, H.G., Blair, S.S., 2006. Shaping BMP morphogen gradients in the Drosophila embryo and pupal wing. Development 133, 183-193.

O'Grady, P.M., Kidwell, M.G., 2002. Phylogeny of the subgenus sophophora (Diptera: drosophilidae) based on combined analysis of nuclear and mitochondrial sequences. Mol Phylogenet Evol 22, 442-453.

Osterfield, M., Du, X., Schupbach, T., Wieschaus, E., Shvartsman, S.Y., 2013. Three-dimensional epithelial morphogenesis in the developing Drosophila egg. Dev Cell 24, 400-410.

Parchem, R.J., Perry, M.W., Patel, N.H., 2007. Patterns on the insect wing. Current opinion in genetics & development 17, 300-308.

Parker, L., Stathakis, D.G., Arora, K., 2004. Regulation of BMP and activin signaling in Drosophila. Prog Mol Subcell Biol 34, 73-101.

Parks, S., Wakimoto, B., Spradling, A., 1986. Replication and expression of an X-linked cluster of Drosophila chorion genes. Dev Biol 117, 294-305.

Peri, F., Bokel, C., Roth, S., 1999. Local Gurken signaling and dynamic MAPK activation during Drosophila oogenesis. Mech Dev 81, 75-88.
Peri, F., Roth, S., 2000. Combined activities of Gurken and decapentaplegic specify dorsal chorion structures of the Drosophila egg. Development 127, 841-850.

Pfeiffer, B.D., Jenett, A., Hammonds, A.S., Ngo, T.T., Misra, S., Murphy, C., Scully, A., Carlson, J.W., Wan, K.H., Laverty, T.R., Mungall, C., Svirskas, R., Kadonaga, J.T., Doe, C.Q., Eisen, M.B., Celniker, S.E., Rubin, G.M., 2008. Tools for neuroanatomy and neurogenetics in Drosophila. Proceedings of the National Academy of Sciences of the United States of America 105, 9715-9720.

Piano, F., Craddock, E.M., Kambysellis, M.P., 1997. Phylogeny of the island populations of the Hawaiian Drosophila grimshawi complex: evidence from combined data. Mol Phylogenet Evol 7, 173-184.

Pyrowolakis, G., Hartmann, B., Muller, B., Basler, K., Affolter, M., 2004. A simple molecular complex mediates widespread BMP-induced repression during Drosophila development. Dev Cell 7, 229-240.

Queenan, A.M., Ghabrial, A., Schupbach, T., 1997. Ectopic activation of torpedo/Egfr, a Drosophila receptor tyrosine kinase, dorsalizes both the eggshell and the embryo. Development (Cambridge, England) 124, 3871.

Ray, R.P., Schupbach, T., 1996. Intercellular signaling and the polarization of body axes during Drosophila oogenesis. Genes & development 10, 1711-1723.

Reeves, G.T., Muratov, C.B., Schupbach, T., Shvartsman, S.Y., 2006. Quantitative models of developmental pattern formation. Dev Cell 11, 289-300.

Ruohola-Baker, H., Grell, E., Chou, T.B., Baker, D., Jan, L.Y., Jan, Y.N., 1993. Spatially localized rhomboid is required for establishment of the dorsal-ventral axis in Drosophila oogenesis. Cell 73, 953-965.

Sapir, A., Schweitzer, R., Shilo, B.Z., 1998. Sequential activation of the EGF receptor pathway during Drosophila oogenesis establishes the dorsoventral axis. Development 125, 191-200.

Schwank, G., Dalessi, S., Yang, S.-F., Yagi, R., Morton De Lachapelle, A., Affolter, M., Bergmann, S., Basler, K., 2011. Formation of the long range Dpp morphogene gradient. PLoS Biol 9, e1001111. doi:1001110.1001371/journal.pbio.1001111.

Shilo, B.Z., 2005. Regulating the dynamics of EGF receptor signaling in space and time. Development 132, 4017-4027.

Shravage, B.V., Altmann, G., Technau, M., Roth, S., 2007. The role of Dpp and its inhibitors during eggshell patterning in Drosophila. Development 134, 2261-2271.

Sopko, R., Perrimon, N., 2013. Receptor tyrosine kinases in Drosophila development. Cold Spring Harbor perspectives in biology 5.

Spradling, A.C., 1981. The organization and amplification of two chromosomal domains containing Drosophila chorion genes. Cell 27, 193-201.

Spradling, A.C., 1993. Developmental genetics of oogenesis. In: *The Development of Drosophila melanogaster*. Plainview: Cold Spring Harbor Laboratory Press.

Tamura, K., Peterson, D., Peterson, N., Stecher, G., Nei, M., Kumar, S., 2011. MEGA5: molecular evolutionary genetics analysis using maximum likelihood, evolutionary distance, and maximum parsimony methods. Mol Biol Evol 28, 2731-2739.

Thio, G.L., Ray, R.P., Barcelo, G., Schupbach, T., 2000. Localization of gurken RNA in Drosophila oogenesis requires elements in the 5' and 3' regions of the transcript. Dev Biol 221, 435-446.

Tolias, P.P., Konsolaki, M., Halfon, M.S., Stroumbakis, N.D., Kafatos, F.C., 1993. Elements controlling follicular expression of the s36 chorion gene during Drosophila oogenesis. Mol Cell Biol 13, 5898-5906.

Turing, A.M., 1952. The Chemical Basis of Morphogenesis. Philosophical Transactions of the Royal Society of London 237, 37-72.

Twombly, V., Blackman, R.K., Jin, H., Graff, J.M., Padgett, R.W., Gelbart, W.M., 1996. The TGF-beta signaling pathway is essential for Drosophila oogenesis. Development 122, 1555-1565.

Van Buskirk, C., Schupbach, T., 1999. Versatility in signalling: multiple responses to EGF receptor activation during Drosophila oogenesis. Trends in cell biology 9, 1-4.

Van Buskirk, C., Schupbach, T., 2002. Half pint regulates alternative splice site selection in Drosophila. Dev Cell 2, 343-353.

Vuilleumier, R., Springhorn, A., Patterson, L., Koidl, S., Hammerschmidt, M., Affolter, M., Pyrowolakis, G., 2010. Control of Dpp morphogen signalling by a secreted feedback regulator. Nat Cell Biol 12, 611-617.

Wang, P.Y., Chang, W.L., Pai, L.M., 2008. Smiling Gurken gradient: An expansion of the Gurken gradient. Fly 2, 118-120.

Wang, X., Bo, J., Bridges, T., Dugan, K.D., Pan, T.C., Chodosh, L.A., Montell, D.J., 2006. Analysis of cell migration using whole-genome expression profiling of migratory cells in the Drosophila ovary. Dev Cell 10, 483-495.

Ward, E.J., Berg, C.A., 2005. Juxtaposition between two cell types is necessary for dorsal appendage tube formation. Mech Dev 122, 241-255.

Waring, G.L., 2000. Morphogenesis of the eggshell in Drosophila. Int Rev Cytol 198, 67-108.

Wolpert, L., 1969. Positional information and the spatial pattern of cellular differentiation. Journal of theoretical biology 25, 1-47.

Wu, M.Y., Hill, C.S., 2009. Tgf-beta superfamily signaling in embryonic development and homeostasis. Dev Cell 16, 329-343.

Yakoby, N., Bristow, C.A., Gong, D., Schafer, X., Lembong, J., Zartman, J.J., Halfon, M.S., Schupbach, T., Shvartsman, S.Y., 2008a. A combinatorial code for pattern formation in Drosophila oogenesis. Dev Cell 15, 725-737.

Yakoby, N., Lembong, J., Schupbach, T., Shvartsman, S.Y., 2008b. Drosophila eggshell is patterned by sequential action of feedforward and feedback loops. Development 135, 343-351.

Zartman, J.J., Cheung, L.S., Niepielko, M.G., Bonini, C., Haley, B., Yakoby, N., Shvartsman, S.Y., 2011. Pattern formation by a moving morphogen source. Physical biology 8, 045003.

Zartman, J.J., Kanodia, J.S., Cheung, L.S., Shvartsman, S.Y., 2009. Feedback control of the EGFR signaling gradient: superposition of domain-splitting events in Drosophila oogenesis. Development 136, 2903-2911.